Anal Bioanal Chem (2016) 408:2839–2859
DOI 10.1007/s00216-015-9210-4

REVIEW

Recent development and application of cataluminescence-based sensors

Zi Long[1] · Hong Ren[1] · Yuhan Yang[1] · Jin Ouyang[1] · Na Na[1]

Received: 30 September 2015 / Revised: 15 November 2015 / Accepted: 20 November 2015 / Published online: 29 December 2015

Abstract A cataluminescence (CTL)-based sensor is fabricated based on the CTL signals generated from catalytic reaction on the surface of solid catalytic materials. CTL-based sensors have been developed since the 1990s and have attracted extensive attention due to long-term stability, linear concentration dependence, good reproducibility and fast response. In recent years, CTL-based sensors and sensor arrays have played important roles in chemical analysis, and were applied to determine the presence of organic gas, inorganic gas, or biological molecules, or to evaluate catalysts. However, due to the relatively low catalytic ability of catalysts or low reactivity of some analytes, high working temperature was normally adopted, which limited the applications. Recently, more advanced techniques were introduced into the fabrication of CTL-based sensors to increase the range of applications, such as advanced enrichment techniques, advanced sampling methods, advanced assisted devices, or multiple detections in array or tandem forms. This review summarizes the recent advancements of CTL-based sensors on development of advanced equipment, advanced sensing materials, new working principles examination, and new applications. Finally, we discuss some critical challenges and prospects in this field.

Published in the topical collection featuring *Young Investigators in Analytical and Bioanalytical Science* with guest editors S. Daunert, A. Baeumner, S. Deo, J. Ruiz Encinar, and L. Zhang.

✉ Na Na
nana@bnu.edu.cn

[1] Key Laboratory of Theoretical and Computational Photochemistry, College of Chemistry, Beijing Normal University, Beijing 100875, China

Keywords Cataluminescence (CTL) · Sensor · Enrichment · Room-temperature sensing · Plasma-assisted sensor array · Tandem CTL

Introduction

In 1976, Michèle Breysse and co-workers observed a specific luminescence during the catalytic oxidation of carbon monoxide on thoria surface [1]. They proposed that this kind of luminescence was not the previously observed adsorbluminescence but the light emission originating from the annihilation of excitons produced during the catalytic reaction of adjacent O species and CO^+ [2], and it was named as cataluminescence (CTL). Normally, CTL refers to the emission of electromagnetic radiation generated from the catalytic oxidation on the surface of solid materials. The signal intensity is in proportion to the catalysis rate of gas [3], which indicates that the CTL signals could be used to fabricate sensors for gas detection. Nevertheless, in the early days, researchers paid more attention to the adsorption and intermediates during catalytic reaction, and CTL-based sensors were not widely used to determine gases [4].

Then, in 1990, Nakagawa et al. made an effort to explain the origins of the band spectra observed on the surface of the heating bulk γ-Al_2O_3 when ethanol vapor passed through [5]. Subsequently, a series of simply equipped CTL-based sensors were designed to detect gaseous acetone, ethanol, butanol, butyric acid, as well as odor substances, catalytic materials of which were bulk solid such as γ-Al_2O_3 [6–9], Dy^{3+} [10], or Dy_2O_3 [11] doped γ-Al_2O_3. They also applied temperature cycle techniques to detect each component in mixed gas samples by counting the entire CL signals in the warming and cooling period. Significantly, there was an exactly linear relation between the gas content and CTL intensity, which was the

essential assurance to the fabrication of a CTL-based sensor. These are monumental studies for CTL-based sensors.

In the 21st century, with the rapid development of nanotechnology, nanosized solid materials received widespread attentions. Zhang's group selected nanosized TiO_2 as the sensing material to detect organic gas [12], which was considered as a pioneering work for the combination of nanomaterials and CTL for sensing. Since then, with the adoption of various nanocatalysts, including nano-oxides, nano-carbonates and the nano-composites for CTL reactions, CTL-based sensor became more sensitive, selective, miniaturized, and efficient in chemical analysis because of the larger surface area and diverse structures of nanocatalysts. Meanwhile, due to the relative low catalytic ability of catalysts or low reactivity of some analytes, several-hundred-degree working temperature was normally adopted, which limited the applications with low performance. Then, more breakthroughs have been introduced for the development of sensors, such as the dielectric barrier discharge technique for analyte activation [13–16], and the headspace solid-phase microextraction (HS-SPME) technology [17] for sample enrichment. Moreover, sensor arrays emerged based on the cross-reactive signals of different detection targets on different catalysts in the development process of CTL-based sensors [18]. With the multifarious nanocatalysts and improved equipment, CTL-based sensor has turned out to be a promising transducer, achieving the following breakthroughs: (1) the types of analytes have dramatically expanded from gases or volatile organic substances to aqueous samples such as saccharides, proteins, and even cells. (2) The temperature of sensing system decreased greatly from hundreds of degrees Celsius to less than 100 °C and even to room temperature. (3) The sensing mechanism became clearer based on the experimental and calculation results. After several years of development, CTL-based sensor shows significant advantages like fast response, linear concentration dependence, long time stability, excellent reproducibility, and high sensitivity. In this review, we focus on the recent advances on CTL-based sensors on working principles, developed equipments, diverse sensing materials, and novel applications.

Working principles of CTL

The examinations on working principles are significant for designing new sensing systems, optimizing working conditions, and improving the performance of sensors. CTL is generated in the process of heterogeneous catalytic reactions on the surface of solid materials. The overall reaction proceeds through five steps as Fig. 1 illustrates [19], which are:

(1) Reactant (R) and oxygen (O) diffuse from the outer gas phase, arrive at the catalyst surface.

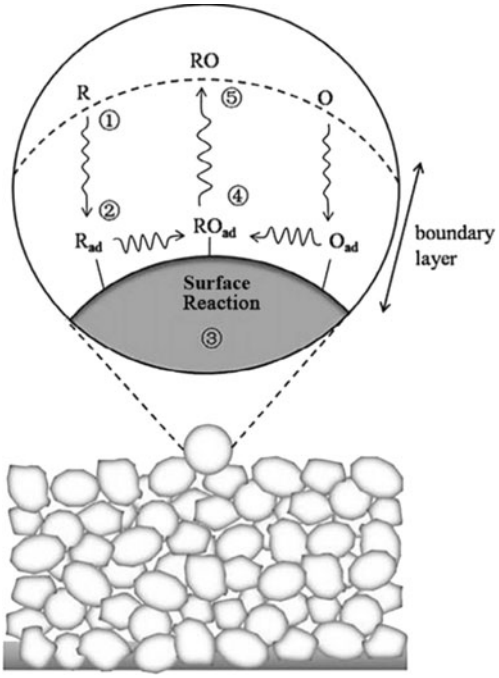

Fig. 1 Schematic of overall reaction processes on the catalyst surface

(2) R and O are chemisorbed to form R_{ad} and O_{ad} at the surface of catalyst. Meanwhile, some adsorbates are desorbed to the gas phase again.
(3) R_{ad} and O_{ad} react to form chemisorbed RO_{ad} at the surface.
(4) The product RO is desorbed from the surface.
(5) RO diffuses off to the gas phase.

Traditionally, there are two developed views to account for the emission; one is the radiation from the excited species and the other is the recombination radiation [19]. The former viewpoint considers that the luminescence is generated from the photon release during the produced excited species falling to the ground state. As for the latter viewpoint, it is believed that the desorption of RO_{ad} is coupled with annihilation of the excitons, the recombination of electron and hole resulting in luminescence. Moreover, with the advent of rare-earth ions-doped materials to fabricate CTL-based sensors, an energy-transfer cataluminescence (ET-CTL) mechanism was first presented by Okabayashi et al. [10]. They measured an extra CTL spectrum during the catalytic oxidation of hydrocarbon gas on γ-Al_2O_3 doped Dy^{3+} catalyst, but no emission obtained from γ-Al_2O_3. Similar phenomena were observed in other reports [20, 21]. The ET-CTL mechanism indicates that the energy transfer occurs between the excited intermediates and ions like Dy^{3+} and Eu^{3+} doped in catalyst; the ions would likely catch the energy of excited species if they have matching energy structures and then release it as light [21, 22].

In the course of CTL, the rate of photon emission was related to the generation rate of excited intermediates or

chemisorption surface state [3], which might be affected by the working temperature. Therefore, the working temperature has effect on CTL intensities, which has been proven by previous works [23]. During the catalytic reaction of ethanol and acetone on γ-Al_2O_3 catalyst, researchers found the CTL intensity increased exponentially along with increasing temperature in the "reaction-control region," yet declined sharply when reaching a peak value, indicating the catalytic oxidation came into the "diffusion-control region." Hence, they concluded that the CTL intensity had positive dependence on temperature when it was below the critical temperature, while showing an opposite trend above the critical temperature because of the temperature quenching of CTL emission. CTL intensity of a given sample is proportional to gas content under constant flow rate and at the constant working temperature if the oxygen concentration is high enough; otherwise the intensity will deviate from the linear characteristics.

In addition, another difficulty in mechanism studies is the prediction and identification of excited species. A majority of reports deduced the probable reaction routes through analyzing the exhausted gases of CTL reaction by gas chromatography mass spectrometry (GC-MS) [24–27]. Furthermore, theoretical calculation becomes a powerful tool to predict the intermediates of a typical reaction. Significantly, theoretical calculations can be used for studying CTL mechanism of the catalytic oxidation of ethyl ether, making the reaction route explicit and credible [28].

In a nutshell, the study on CTL working principles paves the way to design CTL-based sensor with high performance. Whatever the type of CTL working principles, CTL intensity depends on the catalytic ability of catalysts, reactivity of analytes, and gas concentration. Thus, creating some novel devices to enrich gas concentration, seeking catalyst with high catalytic ability, and enhancing reactivity of analytes are the key breakthroughs to enhance the sensor's performance.

Instrumentations of CTL-based sensor

Simplicity of instrumentation is one of the most important advantages for CTL sensors. The CTL system consists of five basic parts: (1) a lightproof chamber, (2) a quartz CTL reaction cell with a gas inlet and an outlet, in which a temperature-controlled ceramic chip coated with catalytic materials is placed, (3) a temperature controller for adjusting the chip temperature, (4) an optical filter to select transmittable radiations, and (5) an optical detector, including a photomultiplier, a photon counter, and a computer. Figure 2a shows the basic construction of CTL-based sensor in laboratory [29]. The carrier gas for sending samples is from air pump and the flow rate is controlled by a flow meter, and the typical flow rates often range from 100 to 400 $mL \cdot min^{-1}$. The luminescent signal is recorded by a photomultiplier and then the digitized data were exported as curves. We can get a lot of information about

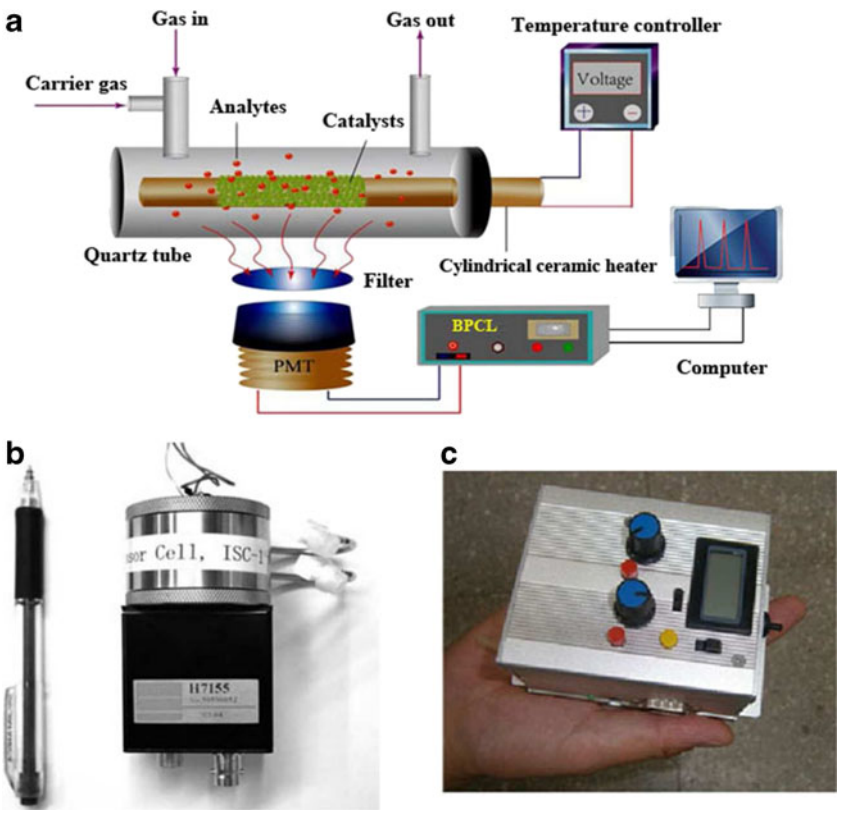

Fig. 2 (**a**) Schematic of the basic construction of CTL-based sensor. (**b**) The appearance of CTL-based sensor cell with a photomultiplier module. (**c**) A photo of a portable CTL-based sensor

samples by analyzing the CTL curves. Figure 2b is a schematic of CTL-based sensor cell with a photomultiplier module designed by Nakagawa [19]. A handheld CTL sensing device is composed of a miniature photomultiplier tube, a miniature gas pump, and a simple light seal (Fig. 2c) [30].

For improving sensitivities and expanding applications, the simple and basic equipment could not meet the demand anymore; some new strategies and techniques were introduced to construct a more efficient sensing system, including (1) sample enrichment technologies, (2) sample introduction techniques, (3) plasma-assisted devices, (4) sensor arrays and imaging systems, (5) tandem CTL techniques and so on. The assisted techniques are listed in Table 1.

Sample enrichment techniques

Enrichment technology is needed because the concentration of analytes in real-life is normally low. As shown in Fig. 3a, a novel CTL-based sensor combined with an ionic liquids (ILs)-based headspace solid-phase microextraction (HS-SPME) technique was applied for quantitative determination of acetones levels in human plasma [17]. ILs could be easily adopted aspseudo-solid carriers for direct loading of acetone into a CTL sensor without substrate interference. As a result, CTL intensity of this kind of sensor improved about 80-fold than the direct injection of the same volume of aqueous samples.

Another case was that nanosized ZrO_2 deposited on a heating filament can be used for the detection of ethanol [31], which acted as both absorbents and catalysts. Ethanol was trapped on ZrO_2 at room temperature and then in-situ detected at a fast elevated temperature. The detection limit for ethanol has improved about 3000-fold compared with the previously techniques using ceramic substrates. Figure 3b shows the key structure of the sensor. Another type of enrichment device is thermal desorption coupled with cataluminescence (TD/CTL) [32], which adopted nano-TiO_2-Y_2O_3 (mass ratio 1:3) as sensing element to determine formaldehyde in air. The concentration of the desorbed formaldehyde in the adsorption tube was much higher than that in air due to the sample accumulation on the surface of adsorbent, so the sensitivity is greatly enhanced. A similar equipment was also developed to detect the trichloroethylene (TCE) gas on ZnO-Y_2O_3 nanocomposites, improving the sensitivity greatly [33]. However, it should be noted that the TD/CTL cannot be operated in continuous monitoring mode, which needs further improvements.

Sample introduction systems

Conventional CTL constructions were suitable for gaseous sample detections, and the detection of aqueous samples was difficult for a long time. Then, some novel aerosol sample introduction systems coupled with CTL detectors appeared for the detection of aqueous samples. For example, the continuous sampling of aqueous samples was achieved by a homemade nebulizer. It was a fused-silica capillary (75-μm i.d., 0.18-mm o.d.) surrounded by a larger tube (0.35-mm i.d., 1.2-mm o.d.) through which filtered and pressurized air was supplied [34]. The angle between the nebulizer and the cylindrical ceramic heater was set as 15° to achieve higher sensitivity (Fig. 4a). The saccharides can be successfully detected with a 70-fold higher sensitivity based on CTL signals on porous alumina than UV absorbance. Furthermore, based on electrospray, a Venturi electrosonic spray ionization (V-ESSI) CTL sensor array was fabricated for discriminating saccharides in solution (Fig. 4b) [35]. It achieved good discrimination of different saccharides and discriminated four groups of urine sugar-level for urine samples from diabetic patients. The sample introduction techniques have enlarged the application field of CTL sensors.

Plasma-assisted devices

For traditional CTL reactions, because of the relative low catalytic ability of catalysts or low reactivity of some analytes, high working temperature was normally adopted, and the detection of analytes with low reactivity (such as hydrocarbons) was hard to achieve [3]. The introducing of non-thermal plasma is a creative method for enhancing CTL performance, which generated by dielectric barrier discharge (DBD) in atmospheric pressure [14]. Non-thermal plasma contains energetic electrons radicals, ions, and metastable species, which can be applied in wide ranges such as ozone generation, surface coating, contamination destruction, or chemical synthesis. Plasma-assisted catalysis (PAC) [16] could give electrons sufficient energy to make molecular bonds rupture, which enabled conventional high-temperature thermally driven reactions to proceed at atmospheric pressure and low temperature. DBD-based CTL system was first used as a BETX sensor [36], and later the improved version was subjected to the fabrication of sensor array for fast discriminations [15]. Figure 5 is the schematic of plasma-assisted CTL- based (PA-CTL) sensor [37]. A copper stick in a tube acted as an electrode, and a piece of copper sheet wrapping the tube as another electrode. The carrier gas and discharge gas (air, N_2, Ar, He) flowed through the tube at a selected flow rate. The plasma probe was generated when an alternating voltage was applied. Based on this equipment, Almasian et al. successfully detected BTEX on nanosized ZrO_2 at lower temperature (190 °C) with higher sensitivity [36]. Our group determined CO at low temperature of about 50 °C on Ag-doped nanocatalyst, and constructed a portable CO sensor with low energy consumption [16]. Recently, room-temperature sensing of CO has been first employed with the Mn-doped alkaline earth nanomaterials as

catalysts [37]. PA-CTL sensors have made great contributions to the development of CTL-based sensor.

Sensor arrays and imaging systems

Conventional CTL-based sensor was usually designed for selective and sensitive detection of single analyte (called "key-to-lock" mode) [38], wherein a specific receptor was applied for strong, highly selective seizing of the specific analyte. However, because of the complexity of the real samples, rapid discrimination of complex samples is urgently needed. A burgeoning strategy that carries forward the traditional chemical sensing method involves the sensor array discrimination. The inspiration of sensor array was from the consummate behaviors of biological mammalian olfactory systems in odors identification, tracking, and location tasks. Sensor array [39], called "electronic noses" or "electronic tongues," has the cross-reactive feature that one receptor responds to various analytes and various receptors respond to any given analyte, creating various signals and providing unique pattern for the identification of individual analyte. Typically, the optical sensor array is used for detecting chemical substances based on changes of optical characteristics, such as signal intensity and wavelength [38, 40–42]. CTL-based sensor array became a highly discernibly tool for quantitative analysis of mixture sample by integrating several sensing materials with different CTL features to form a specific pattern.

It is worth noting that Na and co-workers first constructed a 3 × 3 CTL sensor array and an imaging system by depositing 9 nanocatalysts on a ceramic chip (Fig. 6a) [43]. Gas samples were taken by air passed through the heating sensing units, which initiated different CTL signals on different sites to form specific images (Fig. 6b). Ethanol, H_2S and trimethylamine (TMA) vapors were detected by this sensor array, which showed obvious different signals and the CTL spectrum of each analyte on each nanocatalyst is shown in Fig. 6c. In addition, when the sensor array was exposed to ethanol, H_2S, and TMA, it could be conveniently imaged by a camera and form a unique "fingerprint" according to the luminous spots and the relative CTL brightness, respectively. For a given sample on a sensor array, the brightness of images is influenced by sample concentration and sensing temperature.

Since then, another simple but useful sensor array using a pneumatic nebulizer was designed. As shown in Fig. 7a [44], tiny and homogeneous aerosols containing analytes were generated through pneumatic nebulizer in the chamber. The sensing unit was constructed by sintering nanoparticles on a cylindrical ceramic heater. The CTL signal from each sensing element was recorded by the PMT with orderly injection. Three saccharides, two organic acids, and nine amino acid solutions were discriminated on the sensor array with six sensing materials.

Recently, a CTL-based sensor array was designed for rapid detection and discrimination of flammable liquid (FL) vapors, comprised of 10 catalytic nanoparticles (Fig. 7b) [45]. They directly deposited catalysts on heating filaments to form different sensing elements, and then the obtained sensing units were fixed to the circular Teflon (TPFE) platform. The sensing elements were well separated and the CTL signals from each sensing element were recorded by the PMT in turns to obtain the fingerprints of vapors for discrimination. Combustions originated from the carpet in the presence and absences of gasoline were effectively distinguished by this technique.

Owning to advantages like reversible response, low-cost sensing element, and simple instrumentation, this "electronic nose" has played an important role for real-world "smelling." Furthermore, with the development of nanotechnology, a variety of catalytic materials can be selected as the sensing elements, making the CTL sensor arrays represent a wide range of chemical functionality for the discrimination of different kinds of analytes and the evaluation of catalysts.

Tandem CTL techniques

Furthermore, the tandem CTL techniques can also be used for the discrimination. For example, a novel CTL sensing system composed of two simply connected CTL sensor cells can also be used for recognitions based on the luminescent intensities of the analyte (I_A) and its products (I_R) [46, 47]. As shown in Fig. 8a, the analyte passed through the first sensing element, and the product gases were then regarded as a new reactant passing through a long air pipe to the second sensing material. The CTL signals of I_A and I_R were recorded in a short time using a photomultiplier. Eleven kinds of organic gases were favorably identified using I_A/I_R values, demonstrating the practicability of this sensing system. The tandem CTL sensor is impressive for its high sensitivity and high selectivity.

Sometimes, a single type of signal obtained from an individual transducer is not convincing enough to realize analytes detection; multidimensional information accumulated simultaneously in one sensor is becoming popular. A dual-channel sensing system based on the electrical and optical properties of SnO_2 nanocatalyst was designed for the discrimination (Fig. 8b) [48]. Two-dimensional information including conductivity change of catalyst and CTL signals on tin oxide nanoparticles were obtained during CTL reactions. The optical-electrical sensing system is expected to construct a multifunctional sensor array for identification and discrimination of complicated samples with higher accuracy.

Sensing materials

Sensing material is a core unit of the CTL-based sensor system, which will affect sensitivity, selectivity, and

Table 1 Assisted techniques of CTL sensing systems

	Analytes	Catalysts	Optimal conditions (wavelength, temp., flow rate)	LOD	Assisted technique	Ref
HPLC/CE detector	Acetone in human plasma	Nanosized Al_2O_3	–	3 μL	An ionic liquid-based headspace solid phase (HS-SPME) device	[17]
	Saccharides	Nanosized porous Al_2O_3	460 nm, 400 °C, 14 $dm^3 \cdot min^{-1}$	–	An aerosol CTL based detector	[49]
	Saccharides	Nanosized porous Al_2O_3	460 nm, 450 °C, 200 $\mu L \cdot min^{-1}$	–	A postcapillary nebulizer	[34]
	Ether, acetone, chloroform, toluene, 2-butanone and acetic anhydride	Nano-sized metal oxides, decorated nanoparticles and carbonates	–	7.4 $\mu g \cdot mL^{-1}$ on MgO for xylose	A Venturi electrosonic spray ionization (V-ESSI) CTL sensor array	[35]
Enrichment technologies coupled to CTL based sensor	Wine identification	Nano-ZrO_2	425 nm, 350 °C	–	A closed reaction cell (CRC)	[50]
	12 medicines and 4 organic gases	MgO and ZrO_2	–	–	A closed reaction cell	[51]
	2-propanol	ZrO_2 nanoparticles	180 °C	11 ppbv	In-situ preconcentration	[52]
	Formaldehyde	Nanosized $Mo_4V_6Ti_{10}O_{47}$	575 nm, 260 °C, 145 $mL \cdot min^{-1}$	0.02 $mg \cdot m^{-3}$	A thermal desorption coupled with CTL (TD/CTL) sensor	[53]
	Formaldehyde	TiO_2-Y_2O_3	490 nm, 195 °C, 280 $mL \cdot min^{-1}$	0.01 $mg \cdot m^{-3}$	A TD/CTL sensor	[32]
	Acetone	Nano-Cr_4TiO_8	430 nm, 366 °C, 115 $mL \cdot min^{-1}$	1.2 $mg \cdot m^{-3}$	A TD/CTL sensor	[54]
	n-Hexane	Y_2O_3-Al_2O_3	400 nm, 200 °C, 300 $mL \cdot min^{-1}$	0.4 $mg \cdot m^{-3}$	A TD/CTL sensor	[55]
	Trichloroethylene	ZnO-Y_2O_3	440 nm, 210 °C, 70 $mL \cdot min^{-1}$	4.9 $mg \cdot m^{-3}$	A TD/CTL sensor	[33]
Plasma assisted CTL (PA-CTL)	Acetic acid	Nano/micro CuO/ZnO	295 °C, 600 $mL \cdot min^{-1}$	3 $mg \cdot L^{-1}$	A dielectric barrier discharge device	[56]
	BETX	Nanosized ZrO_2	150-250 °C	20 ng	A plasma-assisted CTL sensor	[36]
	CO	Ag doped alkaline-earth nanomaterials	50 °C	43 ppm	A plasma-assisted CTL sensor	[16]
	Xylene isomers	Nano-Y_2O_3, γ-Al_2O_3, ZrO_2	–	33 $ng \cdot mL^{-1}$ for CH_4: on MgO	A plasma-assisted CTL sensor	[57]
	CO	Mn/SiO_2 nanomaterials	Room temperature	20 ppm	Non-thermal plasma assisted (NTPA) catalysis system	[37]
	Gaseous hydrocarbons	Alkaline-earth nanomaterials	CH_4 : 33 $ng \cdot mL^{-1}$ on MgO	–	A 4 × 3 plasma-assisted CTL sensor array	[15]
Hyphenated techniques	VOCs	MgO and $SrCO_3$	400 nm, 250 °C, 280 $mL \cdot min^{-1}$	–	Two simple tandem CTL sensor cells	[46]
	20 VOCs	Nanosized SnO_2	–	–	A novel dual channel sensing method based on electrical and optical signals.	[58]

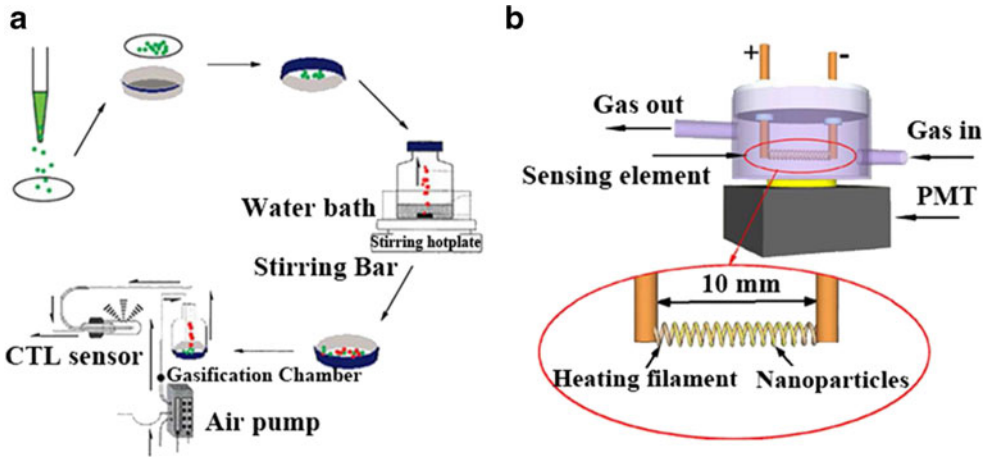

Fig. 3 (**a**) Schematic of headspace solid-phase microextraction (HS-SPME)-CTL setup coupled with direct solid-support sample loading. (**b**) In-situ enrichment and CTL detection system

stability of the sensors. Sensing materials with high catalytic activity can accelerate the reaction rate, expand the detection range, and lower the working temperature, thus enhancing the performance of sensor. The sizes of sensing materials underwent the development from bulk to nanometer; the components of catalysts experienced the development from pure mater to the complex; the morphology of catalytic material developed from powder, sheet to crystalline and nanoparticle.

We named the early development of CTL-based sensor as the bulk solid materials period. To select catalyst for CTL-based sensor, the classic catalyst of γ-Al_2O_3 was used for the detection of combustible gases assisted by temperature-gradient technique at a constant heating and cooling rates of $\pm 9\ °C \cdot s^{-1}$ in a temperature cycle between 200 and 740 °C, which achieved the limit of detection of 1 ppm [6]. Then, Dy^{3+} doped γ-Al_2O_3 was used to determine the fragrance vapors and hydrocarbons with lower LOD and lower working temperature than using single γ-Al_2O_3 [10].

New breakthrough of sensing elements to nanomaterials occurred in 2002 [12], which applied seven nanoparticles, including nanosized-MgO, Y_2O_3, TiO_2, $LaCoO_3$:Sr^{2+}, Al_2O_3, $SrCO_3$, and ZnO to detect organic vapors. After the evaluation based on CTL signals, nanosized TiO_2 was first chosen as the sensor substrate for fabricating a CTL detector, relying on its good stability, high activity, and a UV absorption partially overlapping the solar spectrum. The linear ranges were 20–200 $\mu g \cdot mL^{-1}$ for acetone and 40–400 $\mu g \cdot mL^{-1}$ for ethanol, and the LOD was lower than 10 $\mu g \cdot mL^{-1}$. This has revealed a pathway for the application of nanomaterilas into CTL-based sensors.

From then on, many research groups devoted their efforts to seek high performance nanocatalysts based on nanosized catalysts' larger surface areas and higher selectivity than bulk materials. We called it the nanosized material period. The types of nanomaterials consist of nanometal oxides, carbonates, sulfates, rare metal ions doped nanocomposites, carbon nanotube loaded metal oxide nanocomposites, and so on. The morphology of nanomaterials can be categorized into nanoparticles, nanotubes, microspheres, nanorods, nanoporous, nano-thin films, nanoflower, nano rices, and so on. In the present review, we made a simple summary of nanosized materials for the fabrication of CTL-based sensor. Various types of materials and analytes are listed in Table 2.

According to Table 2, we can abtain some advances in the nanosized material period as follows:

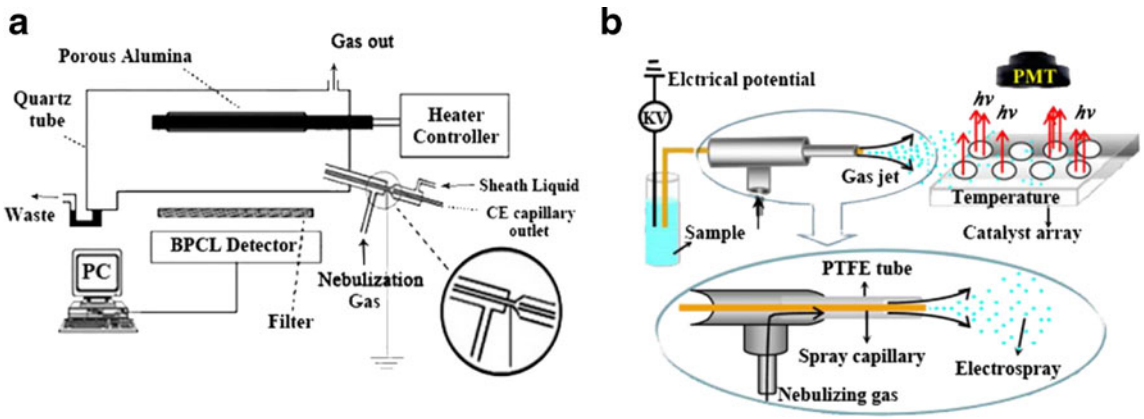

Fig. 4 (**a**) Schematic of the aerosol cataluminescence detection system. (**b**) Schematic of a V-ESSI CTL sensor array

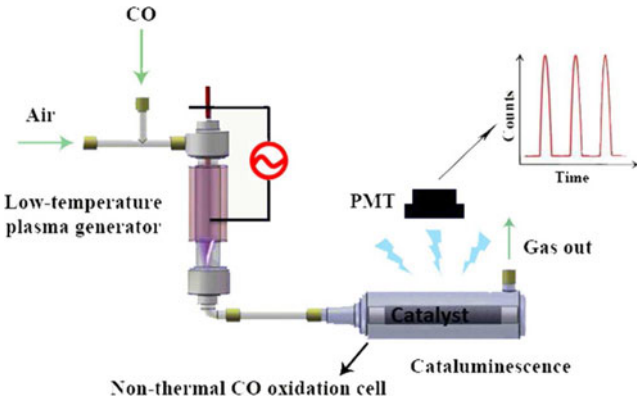

Fig. 5 Schematic of plasma-assisted CTL (PA-CTL) sensor

(1) Bulk materials not expected to act as catalysts show high catalytic activities when they are at nanometer sizes, such as $SrCO_3$, MgO, ZnO, ZnS, $MgSiO_3$ [25, 59, 77, 89, 91] etc.

(2) Different response can be obtained on the same catalyst for different organic molecules detection. Nanosized ZrO_2 showed different performance for the detection of propionaldehyde, ethanol, 2-propanol, and dimethylamine in different working conditinons [29, 31, 52, 92]. Likewise, a given analyte could initiate different CTL signals on different catalysts at different temperature. Taking the oxidation of CO as an example, we obtained different responses of CO on Mn/SiO_2, Co_3O_4 nanorods, flower-like CuO nanostructures, and $La_{0.8}Sr_{0.2}MnO_3$ cubes [37, 68, 69, 72].

(3) Various analytes including gases and aqueous samples, such as BTEX, volatile alcohols, amines, alkanes, ketones, aldehydes, ethers, chloromethanes, and saccharides, can be detected.

(4) The same composition of catalysts with different morphology possessed different catalytic activities. The relations of crystal structure and catalytic activity has been demonstrated in detail [73]. Taking $La_{0.8}Sr_{0.2}MnO_3$ cubes (Cs) and nanoparticles (NPs) for the detection of CO oxidation as an example (Fig. 9a), CTL signals on the two sensing materials demonstrted the higher CTL signals catalyzed by NPs than signals by the Cs before calcination. However, after calcining, the materials with cubic crystalline showed higher CTL intensity and catalytic activity. Catalysts with a high

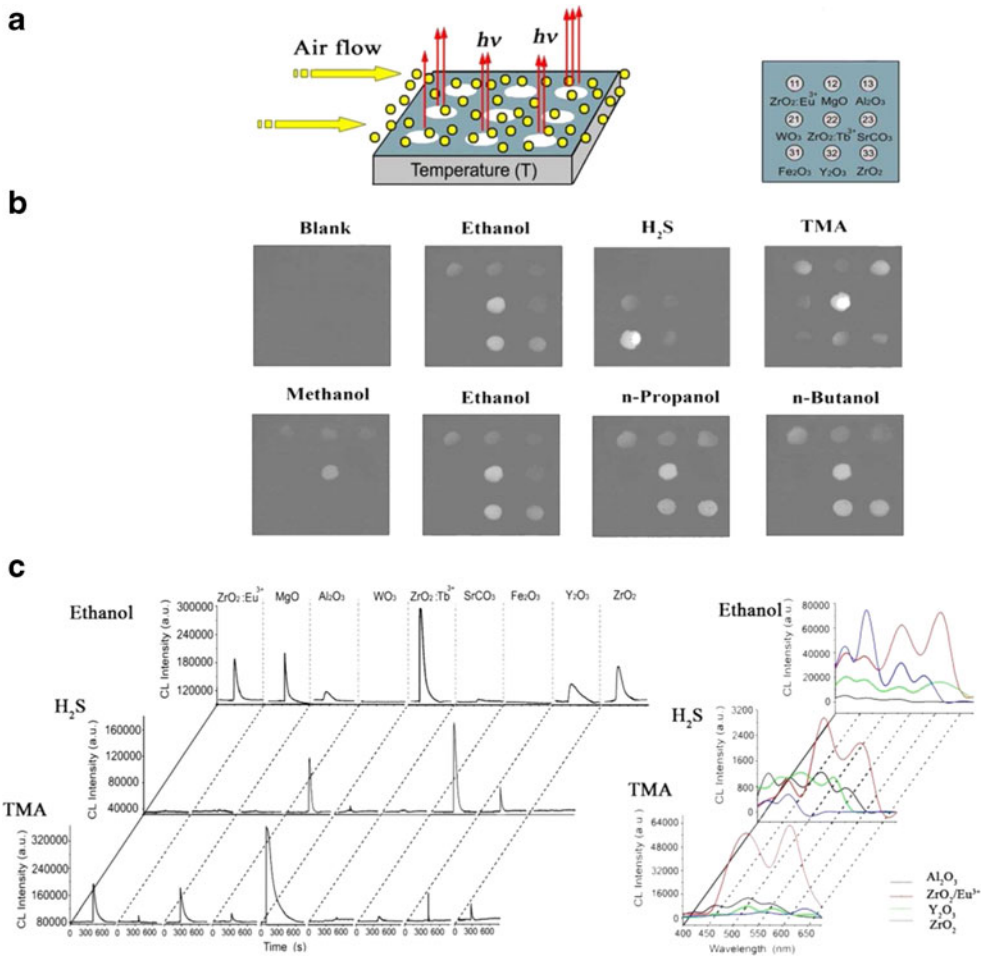

Fig. 6 (**a**) Schematic of the CTL sensor array (left), and the arrangement of nanocatalyst spots (right). (**b**) CTL images of different samples. (**C**) CTL signals (left) and spectra (right) on different nanomaterials

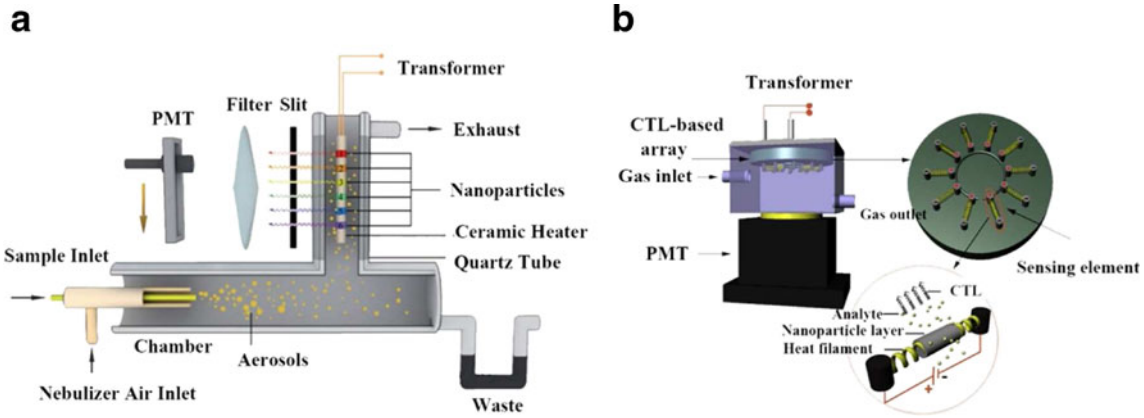

Fig. 7 (**a**) Schematic of CTL sensor array. (**b**) Structural schematic diagram of CTL sensor array

surface area (NPs) could provide more active sites than a small surface area (Cs), which favors the adsorption and activation of the reacting molecules. A similar conclusion was obtained from the comparison of controllably synthesized Mn_3O_4 micro-octahedra and hexagonal nanoplates for acetone determination [78], which showed that Mn_3O_4 micro-octahedra was a better choice because of the catalyst's higher stability and strong CTL intensity than hexagonal nanoplates.

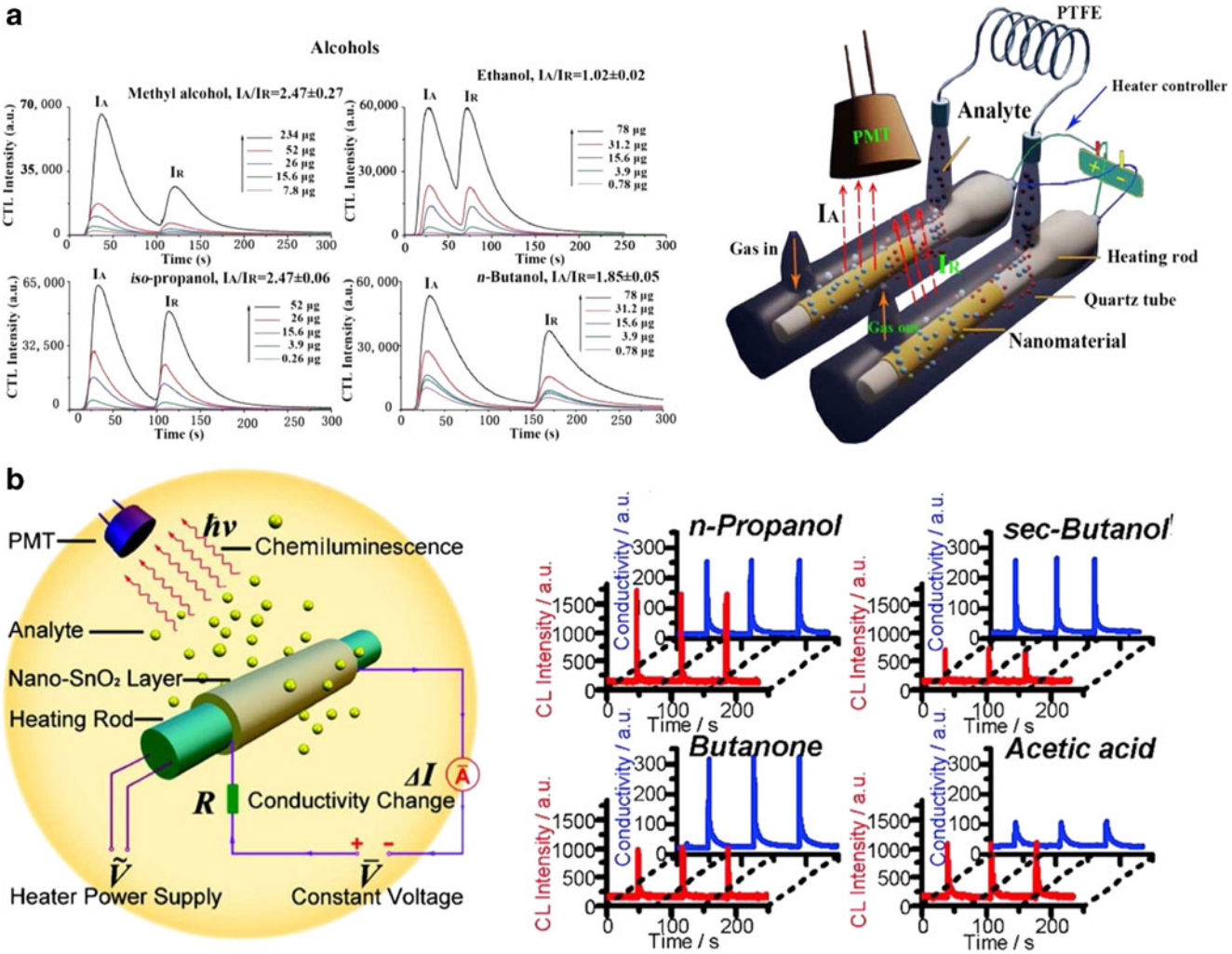

Fig. 8 (**a**) CTL signals by two connected CTL sensors (left) and the principle diagram of the connected tandem CTL system (right). (**b**) Illustration of the dual-channel (conductivity change and CTL emission) sensor (left), and two responses of conductivity and CTL (right)

Table 2 Various sensing materials and analytes of CTL-based sensors

Catalysts	Analytes	Optimal conditions (wavelength, temp., flow rate)	Liner range	LOD	Ref
Period I Bulk solid materials					
ThO_2	CO oxidation	–	–	–	[1]
γ-Al_2O_3	Organic molecules	430–470 nm, 450 °C	1–500 ppm	1.0 ppm	[23]
γ-Al_2O_3:Dy^{3+}	Hydrocarbons	450 °C	0.2–1000 ppm	0.2 ppm	[10]
γ-Al_2O_3 + Dy_2O_3	Fragrance vapors	580, 480, 420 nm, 100–700 °C	0.1–1 ppm		[11]
Period II Nanosized materials					
Nanosized Ag_2Se	CCl_4	460 nm, 240 °C, 250 mL · min^{-1}	0.9–228 μg · mL^{-1}	0.3 μg · mL^{-1}	[58]
Al_2O_3 nanowires	Pinacolyl alcohol	460 nm, 340 °C, 80 mL · min^{-1}	0.09–2.56 μg · mL^{-1}	0.0053 μg · mL^{-1}	[60]
Al_2O_3	Acetone biomarker	–	–	3 μL	[17]
Nanosized Al_2O_3	Saccharides	460 nm, 400 °C, 14 dm^3 · min^{-1}	Glu:10–1000 μg · mL^{-1}	Glu: 3.1 μg · mL^{-1}	[49]
Nanosized Al_2O_3	Saccharides	460 nm, 450 °C, 200 μL · min^{-1}	Glu:30–2000 mg · L^{-1}	Glu: 2.7 μg · mL^{-1}	[34]
Au/layered double hydroxides	Acetaldehyde	105 °C, 400 mL · min^{-1}	1.0–150 mM	0.5 mM	[61]
Nnosized $BaCO_3$	Acetaldehyde	555 nm, 225 °C, 120 mL · min^{-1}	2–2000 ppm	0.5 ppm	[62]
CdO nanostructure	Acetone Diethyl ether	420 nm, 270 °C 450 nm, 285 °C, 240 mL · min^{-1}	8–3000 ppm 10–4000 ppm.	6.5 ppm 6.7 ppm	[63]
CdO nanostructure	Diethyl ether	450 nm, 285 °C, 240 mL · min^{-1}	10–4000 ppm	6.5 ppm	[64]
Nanosized CdS	Alcohols	575 nm, 330 °C, 250 mL · min^{-1}	1.2–76.1 μg · mL^{-1}	0.5 μg · mL^{-1}	[65]
Nanosized CeO_2	CS_2	460 nm, 282 °C, 600 mL · min^{-1}	0.9–12.6 μg · mL^{-1}	3.7 ng · mL^{-1}	[66]
CeO_2 nanoparticles	1,2-Propylene oxide	490 nm, 196 °C, 200 mL · min^{-1}	10–150 ppm	0.9 ppm	[67]
Co_3O_4 nanorods	CO	–	–	–	[68]
Flower-like CuO	CO	425 nm, 200 °C, 100 mL · min^{-1}	–	–	[69]
Nanosized Cr_4TiO_8	Acetone	430 nm, 366 °C, 115 mL · min^{-1}	2.5-150 mg · m^{-3}	1.2 mg · m^{-3}	[54]
Nanosized Fe_2O_3	H_2S	400 nm, 320 °C, 180 mL · min^{-1}	8-2000 ppm	3 ppm	[70]
In_2O_3 film	Acetic acid	425 nm, 303 °C, 250 mL · min^{-1}	3.0-2000 ppm	2.1 ppm	[71]
$La_{1-x}Sr_xMnO_3$ NPs	CO	649 nm, 280 °C, 320 mL · min^{-1}	5.0-320.0 μg · mL^{-1}	0.5 μg · mL^{-1}	[72]
$La_{0.8}Sr_{0.2}MnO_3$ Cubes	CO	640 nm, 200 °C, 100 mL · min^{-1}	–	–	[73]
Nanosized $LaCoO_3$	NH_3	400 °C, 120 mL · min^{-1}	0.04-10 ppm	0.014 ppm	[74]
Nanosized La_2O_3	Acetone	490 nm, 361 °C, 200 mL · min^{-1}	0.19-140 μg · mL^{-1}	0.08 μg · mL^{-1}	[75]
MgO nanoparticles	Vinyl acetate	425 nm, 331 °C, 400 mL · min^{-1}	2-2000 ppm	1.0 ppm	[76]
MgO thin film	2-Ethoxyethanol 2-Methoxyethanol	425 nm, 279 °C, 300 mL · min^{-1}/210 mL · min^{-1}	2.0-2000 ppm 2.0-1500 ppm	1.0 ppm 1.4 ppm	[77]
Mn_3O_4 micro-octahedra Hexagonal nanoplates	Acetone	284 °C, 500 mL · min^{-1}	2.6-52.2 μg · mL^{-1} 52.2-394 μg · mL^{-1}	0.4 μg · mL^{-1}	[78]
Nanosized $Mo_4V_6Ti_{10}O_{47}$	Formaldehyde	575 nm, 260 °C, 145 mL · min^{-1}	0.04-78 mg · m^{-3}	0.02 mg · m^{-3}	[53]
Nanosized SiO_2	Ethyl acetate	460 nm, 200 °C, 200 mL · min^{-1}	20-300 ppm	3.0 ppm	[26]
Nanosized $SrCO_3$	Ethanol	425 nm, 380 °C,150 mL · min^{-1}	6-3750 ppm	2.1 ppm	[25]

Table 2 (continued)

Catalysts	Analytes	Optimal conditions (wavelength, temp., flow rate)	Liner range	LOD	Ref
TiO_2 nanoparticles	Oxygen Vacancies	–	–	–	[79]
Nanosized TiO_2	CCl_4	220 °C, 40 mL · min^{-1}	0.1-380 ppm	40 ppb	[80]
Nanosized TiO_2	Ethanol Acetone	535 ± 10 nm, 380 °C, 100 mL · min^{-1}	40-400 μg · mL^{-1} 20–200 μg · mL^{-1}	10.5 μg · mL^{-1} 6.7 μg · mL^{-1}	[12]
Nanosized V_2O_5	Tert-butylmercaptan	460 nm, 351 °C, 500 mL · min^{-1}	5.6-196 μg · mL^{-1}	0.5 μg · mL^{-1}	[81]
Nanosized $V_2Ti_4O_{13}$	Formaldehyde	490 nm, 370 °C, 150 mL · min^{-1}	0.1-40 mg · m^{-3}	0.06 mg · m^{-3}	[82]
Nanosized Y_2O_3	Trimethylamine	555 nm, 320 °C, 120 mL · min^{-1}	60-42,000 ppm	10 ppm	[83]
Nanosized Y_2O_3	Benzene	425 nm, 225 °C, 300 mL · min^{-1}	4-7018 mg m^{-3}	1 mg · m^{-3}	[84]
Nanosized Y_2O_3	Benzaldehyde	425 nm, 180 °C, 250 mL · min^{-1}	1.8-10.8 mg · mL^{-1}	0.90 ng · mL^{-1}	[85]
Nanosized Y_2O_3	Ethyl acetate	425 nm, 264 °C, 120 mL · min^{-1}	2.0-250 ppm 250-6500 ppm	0.5 ppm	[86]
Nanosized Y_2MnO_5	Dimethyl Ether	620 nm, 210 °C, 125 mL · min^{-1}	5-120 mg · m^{-3}	3 mg · m^{-3}	[87]
ZnO nanoparticles	Ethanol	460 nm, 358 °C, 80 mL · min^{-1}	1.0-100 ppm	0.7 ppm	[88]
Hierarchical spheres ZnO	Ethanol	490 nm, 356 °C, 300 mL · min^{-1}	4-400 ppm	–	[89]
Nanosized $ZnWO_4$	Ether	425 nm, 330 °C, 240 mL · min^{-1}	20-3500 ppm	8.7 ppm	[90]
Nanosized ZnS	CCl_4	460 nm, 335 °C, 210 mL · min^{-1}	0.4-114 μg · mL^{-1}	0.2 μg · mL^{-1}	[91]
Nanosized ZrO_2	Dimethylamine	620 nm, 330 °C, 350 mL · min^{-1}	4.71-70.7 μg · mL^{-1}	0.647 μg · L^{-1}	[92]
Nanosized ZrO_2	2-Propanol	180 °C	60-600 ppbv	11 ppbv	[52]
Nanosized ZrO_2	Ethanol	130 °C, 150 mL · min^{-1}	0.001-1.0 mg · L^{-1}	0.1 ppm	[31]
Nanosized ZrO_2	Propionaldehyde	440 nm, 265 °C, 160 mL · min^{-1}	2.5-1300 mg · mL^{-3}	0.6 mg · m^{-3}	[29]
Nanosized ZrO_2	Ethanol	195 °C, 460 ± 10 nm	1.6-160 μg · mL^{-1}	0.6 μg · mL^{-1}	[93]
γ-Al_2O_3/Nd_2O_3	Ethylene dichloride	400 nm, 279 °C, 320 mL · min^{-1}	6-5000 ppm	2 ppm	[94]
γ-Al_2O_3:Tb^{3+}	Isoflurane	488 nm, 600 °C	10-50 ppm	–	[95]
Nanosized γ-Al_2O_3/MgO	Tetrahydrofuran	460 nm, 279 °C, 360 mL · min^{-1}	1.0-3000 mL · m^{-3}	0.67 mL · m^{-3}	[96]
Alkaline-earth metal salts	H_2S	320 °C, 180–200 mL · min^{-1}	25-500 ppm	2 ppm	[97]
Cocoon-like Au/La_2O_3	VOCs	300 °C, 200 mL · min^{-1}	–	–	[98]
Nanosized Au/La_2O_3	Benzene	420 nm, 210 °C, 200 mL · min^{-1}	1-4000 ppm	0.7 ppm	[99]
Boehmite nanococoon	Ethanol	425 nm, 200 mL · min^{-1}	–	0.0156 g · L^{-1}	[100]
CeO_2-CNT composites	Acetone	125 °C	–	21 μg · mL^{-1}	[101]
Nano/micro CuO/ZnO	Acetic acid	295 °C, 600 mL · min^{-1}	6-500 mg · L^{-1}	3 mg · L^{-1}	[56]
α-Fe_2O_3 nanotubes	H_2S	400 nm, 134 °C, 200 mL · min^{-1}	–	–	[102]
α-Fe_2O_3/g-C_3N_4	H_2S	400 nm, 183 °C, 300 mL · min^{-1}	0.88-7.01 g · mL^{-1}	0.5 g · mL^{-1}	[103]
Fe_3O_4/CNT composites	$(NH_4)_2S$	440 nm, 238 °C, 200 mL · min^{-1}	1.4-115 μg · mL^{-1}	0.05 μg · mL^{-1}	[104]
Nanosized Fe_3O_4/SiO_2.	Automobile exhaust	425 nm, 250 °C, 200 mL · min^{-1}	–	–	[105]
In_2O_3 hierarchical hollow microsphere	H_2S	400 °C, 600 mL · min^{-1}	2-20 μg · mL^{-1}	0.5 μg · mL^{-1}	[106]
Nanosized LaF_3-CeO_2	Triethylamine	490 nm, 205 °C, 360 mL · min^{-1}	0.9-54 ppm	0.2 ppm	[107]

Table 2 (continued)

Catalysts	Analytes	Optimal conditions (wavelength, temp., flow rate)	Liner range	LOD	Ref
$LaSrCuO_4$ nanowires	CO oxidation	425 nm, 200 °C, 200 mL · min^{-1}	–	–	[108]
Hollow Mn_3O_4-in-Co_3O_4 and hollow Co_3O_4 microspheres	CO oxidation	180 °C	–	–	[109]
Mn/SiO_2 nanomaterials	CO	Room temperature	30-4000 ppm	20 ppm	[37]
Nanosized MgO/In_2O_3	Dimethyl ether	425 nm, 245 °C, 280 mL · min^{-1}	50-12000 ppm	14 ppm	[110]
Pd/C	CCl_4	144 °C, 100 mL · min^{-1}	4.7-235 μg · mL^{-1}	0.7 μg · mL^{-1}	[111]
SiO_2 nanotubes and nanoparticles	Ethyl acetate	425 nm, 293 °C, 345 mL · min^{-1}	2.0-2000 ppm –	0.85 ppm	[112]
SiO_2/Fe_3O_4	Ether	431 nm, 310 °C, 240 mL · min^{-1}	10-3000 ppm	6.7 ppm	[113]
SnO_2/carbon nanotube	H_2S	160 °C	–	5 ppm	[114]
SnO_2/graphene materials	Methanol	620 nm, 280 °C,150 mL min^{-1}	6.3-88.5 μg · mL^{-1}	5.2 μg · mL^{-1}	[115]
SnO_2:ZnO nanowires	Ethanol Ketones	620 nm, 260 °C, 250 mL · min^{-1}	11.7-204.7 μg · mL^{-1}	11.0 μg · mL^{-1}	[116]
SnO_2/graphene composite	Propanal	300 °C, 300 mL · min^{-1}	1.3-266.7 mg · mL^{-1}	0.3 mg · mL^{-1}	[117]
Mesoporous SnO_2 nanospheres	H_2S	400 nm, 160 °C, 200 mL · min^{-1}	–	5 ppm	[118]
$SrCO_3$/grapheme	n-Propanol	425 nm, 245 °C, 260 mL · min^{-1}	0.2-32 mg · L^{-1}	0.08 mg · L^{-1}	[119]
Coral-like TiO_2/SnO_2 nanoparticles	Benzene Toluene	430 nm/450 nm, 220 °C/270 °C, 240 mL · min^{-1}	8-800 ppm 1–4000 ppm	6.0 ppm 7.8 ppm	[120]
Coral-like Zn-doped SnO_2	2-Butanone	535 nm, 214 °C, 300 mL min1.	2.31-92.57 mg mL^{-1}	0.6 mg mL^{-1}	[121]
Y_2O_3/Al_2O_3	n-Hexane	400 nm, 200 °C, 300 mL · min^{-1}	1.32-132 mg · m^{-3}	0.4 mg · m^{-3}	[55]
$ZnO\text{-}Y_2O_3$	Trichloroethylene	440 nm, 210 °C, 70 mL · min^{-1}	14.7-586 mg · m^{-3}	4.9 mg · m^{-3}	[33]
ZrO_2/CNT composites	Ethanol	440 nm, 195 °C, 200 mL · min^{-1}	–	–	[122]
Other types of catalysts					
Borate glass	Ethyl Ether	460 nm, 245 °C, 500 mL · min^{-1}	0.12-51.7 μg · mL^{-1}	0.04 μg · mL^{-1}	[28]
Ceramic	Dimethyl ether	425 nm, 279 °C, 300 mL · min^{-1}	100-6.0 × 10^3 ppm	80 ppm	[123]
Layered double oxide	Acetone	300 °C, 400 mL · min^{-1}	0.1-16 mM	0.02 mM	[124]
Layered double hydroxide	Mesityl oxide	210 °C, 400 mL · min^{-1}	1.0-50 mM	0.5 mM	[27]
$Zn_3(BTC)_2 \cdot 12H_2O$ and ZIF-8	H_2S	420 nm, 250 °C, 200 mL · min^{-1} 400 nm, 250 °C, 200 mL · min^{-1}	–	4.4 ppm 3.0 ppm	[125]
Y-doped MOF-5	Isobutanol	490 nm, 207 °C, 400 mL · min^{-1}	6.4-80.1 mg · L^{-1}	3.7 mg · L^{-1}	[126]
Co-MOF	L-cysteine	–	0.1-10 μM	18 nM	[127]
Zeolite	Acetaldehyde	460 nm, 230 °C, 150 mL · min^{-1}	0.06-31.2 μg · mL^{-1}	0.02 μg · mL^{-1}	[128]
Zeolite	n-Hexane	460 nm, 225 °C, 200 mL · min^{-1}	0.776-23.28 μg · mL^{-1}	0.155 μg · mL^{-1}	[129]

(5) Catalysts doped by metal ions have significantly different properties from each other in catalytic reactions. Taking the detection of ethanol by YVO_4 and YVO_4:Eu^{3+} luminescent nanocrystals as an example [20], the maximum CTL emission wavelengths were quite different between the two catalysts. Based on the CTL spectra and the fluorescence spectra (Fig. 9b) of YVO_4:Eu^{3+} and YVO_4 nanocrystals, an energy transfer mechanism from the excited species to the YVO_4:Eu^{3+} nanocrystals was proposed to account for the phenomenon. Na's work also discovered that Mn^{2+} doped in SiO_2 with different percentages would cause different CTL signals under constant reaction condition [37].

Besides commonly used nanomaterials, other types of catalysts also emerged in recent years. Zeolite has been used as catalysts for tracing *n*-hexane in air with a detection limit of 0.155 $\mu g \cdot mL^{-1}$ [129]. The luminescent characteristics of acetaldehyde in the cages of large-pore zeolites has also been examined with a linear response range of 0.06–31.2 $\mu g \cdot mL^{-1}$ [128]. It was speculated that the collisional pairs of analytes could be generated in the three-dimensional network, and the adsorption resembled a carbonium ion to strongly stabilize by the lattice of zeolite for the selective detection of acetaldehyde. A Y-doped metal-organic framework (MOF) also acted as a catalyst to sense isobutanol, showing excellent adsorption and catalytic properties [126]. In addition, borate glass and ceramic were used as sensing elements for sensing ethyl ether and dimethyl ether, respectively [28, 123].

Briefly, catalyst plays an important role in expanding the applications of CTL-based sensors. Recent studies demonstrated that chemical composition, particle size, morphology, crystalline structure, and other parameters related to the conditions of material preparation have profound influence on their catalytic properties.

Applications of CTL-based sensor

With the development of sensing materials and improved equipments, the application range of CTL-based sensor has been broadened extensively. Nowadays, CTL-based sensors can be used for detecting gaseous samples as well as the compounds in aqueous solutions such as biomolecules. In addition, CTL-based sensor array can also be applied to evaluate catalysts.

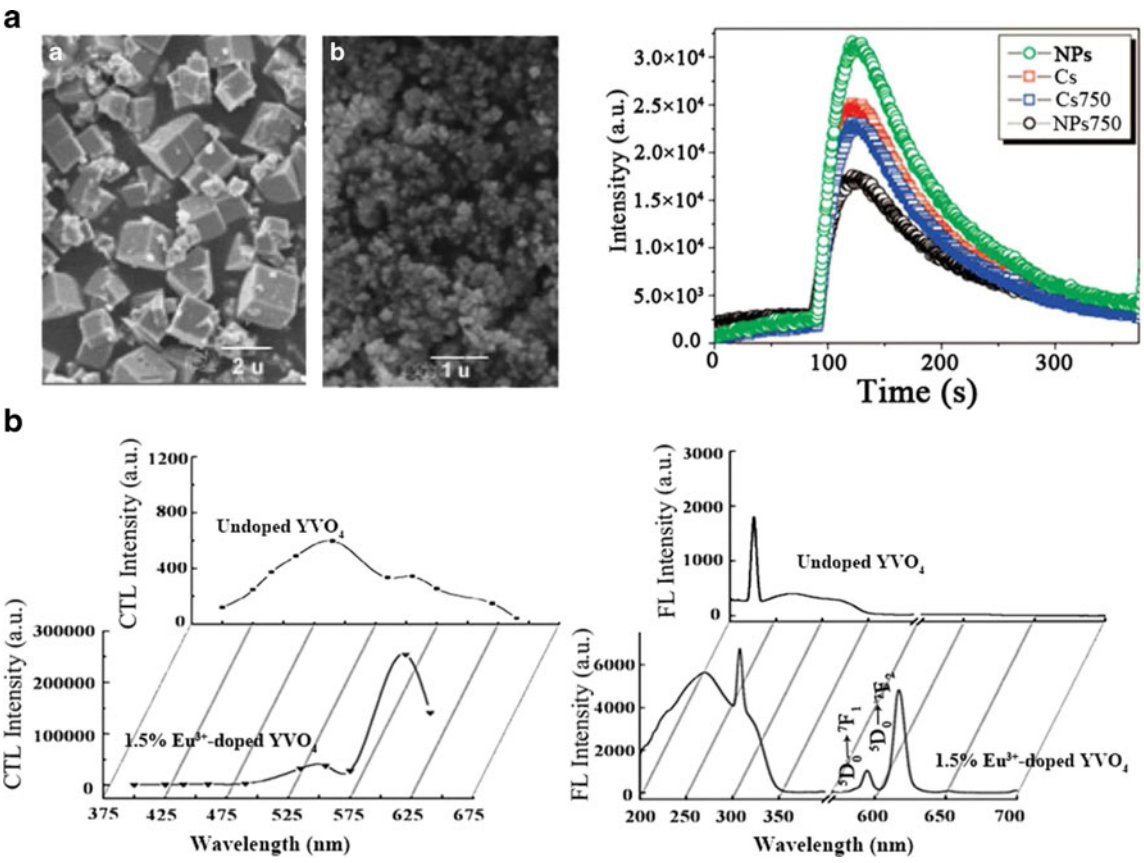

Fig. 9 (**a**) SEM photos of $La_{0.8}Sr_{0.2}MnO_3$ cubes (Cs) (a), the nanoparticles (NPs) (b), CTL spectra of $La_{0.8}Sr_{0.2}MnO_3$ catalysts (right). (**b**) The CTL spectra of ethanol on nanocrystals, and fluorescence emission of nanocrystals for undoped YVO_4 and 1.5 % Eu^{3+}-doped YVO_4. (Cs750 and NPs750: Cs and NPs calcined at 750 °C for 48 h in air, respectively)

Gaseous samples detection

CTL-based sensors can be used for the detection of gaseous samples, including organic gas or volatile organic compounds (VOCs) and inorganic gases. The organic gas or VOCs, such as acetone, ethanol, vinyl acetate, ethyl acetate, formaldehyde, trimethylamine, BETX, propanal, tetrahydrofuran, chloride, pinacolyl alcohol, tert-butyl mercaptan, dimethyl ether, ether, and ethylene dichloride, have been selectively detected by CTL-based sensors or sensor arrays in recent years (Table 2).

Detection of hydrocarbons is a hot topic for CTL sensing. A 4 × 3 plasma-assisted sensor array was fabricated using alkaline-earth nanomaterials as catalysts for fast detecting and discrimination of gaseous hydrocarbons (Fig. 10a) [15]. The characteristic pattern was formed based on strong and unique CTL signals. Considering the different content of hydrocarbons in exhaled breath of healthy and unhealthy people, exhaled breath of healthy people and lung cancer patients were tested. A pretty good discrimination was achieved, which showed great potential in fast clinical diagnosis (Fig. 10b).

Smoking is harmful to our health because of the existence of some pernicious organic molecules. A 3 × 7 CTL-based sensor array composed of 21 catalysts [130] was used to identify the evaporated flavors of different heated tobaccos. The obtained CTL patterns of six brands were distinguishable from each other. This has demonstrated that the sensor array can possibly discriminate closely related odorant compounds if the sensing materials are with high catalytic activities. Also, six drug precursor gases were detected by a 4 × 4 portable embedded gas detection device [131].

In addition, CTL intensity sometimes can be developed as a simple probe for oxygen vacancies in nanoparticles. The CTL intensity of diethyl ether during catalytic oxidation on the surface of TiO_2 nanoparticles is in proportion to the content of oxygen vacancies (Fig. 10c) [79]. The abundant chemisorbed O_2 in oxygen vacancies would react with chemisorbed diethyl ether molecules on the surface of heated catalysts to improve CTL intensity. Judging from the experimental results, there was a corresponding relationship that existed between CTL intensity and amount of oxygen vacancies. Moreover, the CTL intensity of diethyl ether varied with the change of Cu doping content in TiO_2 (Fig. 10d). Therefore, it was assumed that the increase of CTL intensity of diethyl ether on the surface of Cu-doped TiO_2 may generate from an increase in oxygen vacancies.

For inorganic gases, CO, NH_3, H_2S, $(NH_4)_2S$, and CS_2 were detected on Co_3O_4 nanorods, flower-like CuO nanostructures,

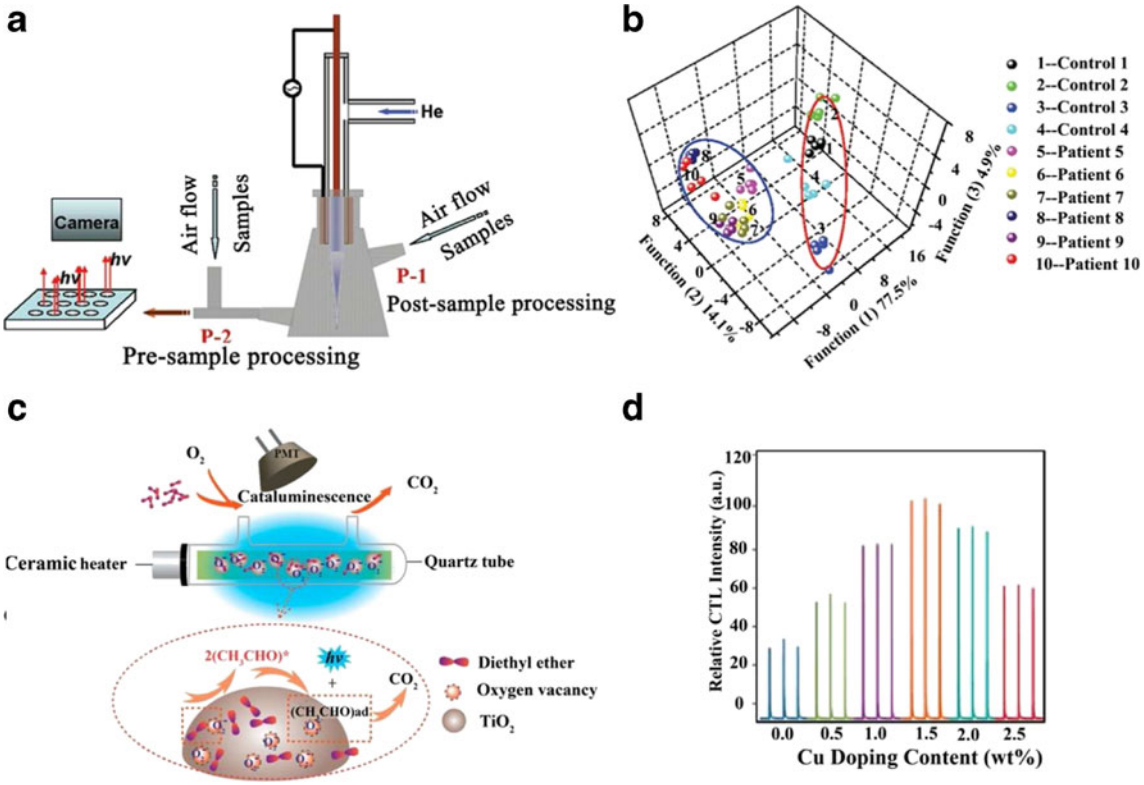

Fig. 10 (**a**) Schematic of the plasma-assisted cataluminescence sensor array. (**b**) The LDA of exhaled breath samples from normal or lung cancerous people (right). (**c**) Schematic of the experimental apparatus for detection of oxygen vacancies. (**d**) Relative CTL signals of 100 mM diethyl ether on the surface of TiO_2 and Cu-doped TiO_2 with different doping contents

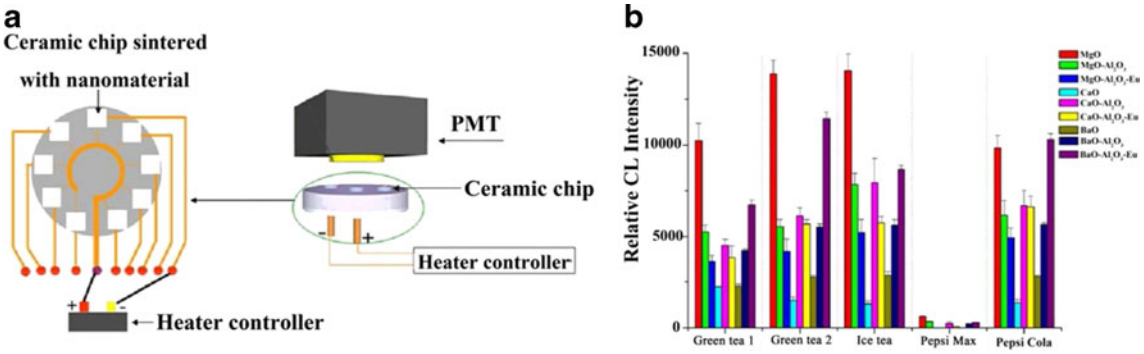

Fig. 11 (**a**) Schematic of a sweeteners recognition CTL-based sensor array. (**b**) CTL intensity histograms of five beverages on the sensor array

α-Fe_2O_3 nanotubes, nano-$TiW_3Cr_2O_{14}$, Fe_3O_4/CNT composites and so on. Thedetails are shown in Tables 1 and 2.

Aqueous sample detection

The detection of aqueous samples by CTL-based method is difficult because the high content of water in solution probably interferes with the analytes, and a high working temperature is needed during the vaporization of aqueous samples [132]. However, in recent years, with the assistance of some improved devices and newly developed nanomaterials, samples detected by CTL-based sensor arrays were not limited to gases but also expanded to aqueous testing samples.

As reported, an original aerosol CTL-based sensor array containing six catalytic nanoparticles used for the pattern recognition of three saccharides, two organic acids, and nine amino acids was proposed [44]. Sample aerosols produced distinct CTL response patterns during the catalytic oxidization, which can be differentiated by linear discriminant analysis (LDA). Eight beverages were successfully discriminated, showing the applicability of this array for real samples. More attractively, the unknown samples at different concentrations can be identified by the training matrix formed by samples at a certain concentration. In addition, a sweeteners-recognition CTL-based sensor array with nine elements was reported (Fig. 11a) [133], which resulted in distinct CTL patterns and well dispersed clusters of five sugars and five artificial sweeteners in aqueous solutions. Moreover, five real

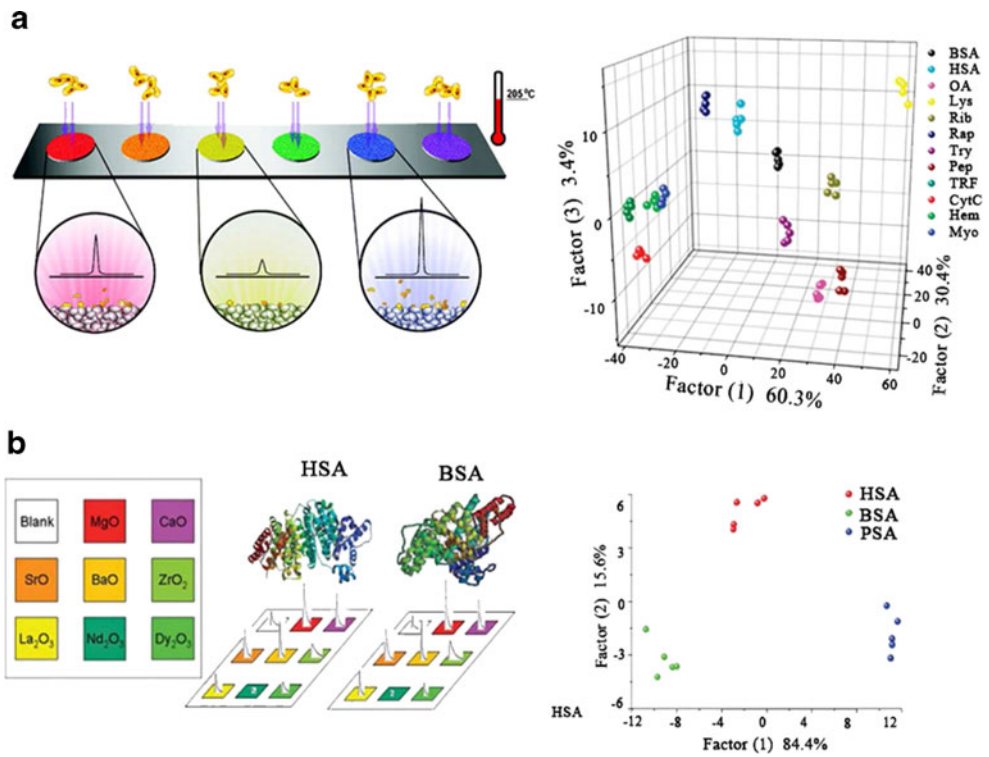

Fig. 12 (**a**) The schematic of the sensing process of TCL, and the LDA result of TCL signals of proteins on the nanomaterials. (**b**) Schematic of the array system for protein discrimination, and LDA result of bovine serum albumin (BSA), human serum albumin (HSA), and porcine serum (PSA)

samples were successfully discriminated based on their CTL signals (Fig. 11b).

A Venturi electrosonic spray ionization (V-ESSI) CTL sensor array has also been used for the discrimination of four groups of urine sugar-level in urine samples from diabetic patients [35], indicating a potential practicality in clinical diagnoses, environment monitoring, food industry, and marine monitoring.

Biomacromolecule detection

The detection of biomacromolecules is much difficult than the gaseous samples as well as the small molecules in solution. This has been overcome by means of thermochemiluminescence (TCL)-based sensor arrays. For example, protein sensing and cell discrimination have been achieved by a TCL-based sensor array (Fig. 12a) [134]. The protein solutions or cell suspensions were directly added on heated ceramics sintered with nanocatalysts, and then the analytes were trapped on the surface of catalysts after the volatilization of water. When the temperatures of nanocatalysts were raised to 205 °C, analytes were thermally oxidized with distinct CTL emission. Four real-life cells containing three cancerous cell lines and one normal cell line were well discriminated. Similarly, researchers further discriminated albumin from human serum (HSA), bovine serum (BSA), and porcine serum (PSA) based on the 'fingerprints' of CTL patterns (Fig. 12b) [135].

Evaluation of catalysts

The catalytic activity of the catalysts greatly affect the CTL intensity, which means that the CTL signals can intuitively reflect catalytic activity of catalysts. Therefore, CTL-based sensors could be applied to evaluate or screen catalysts. A catalysts-screening system was first designed based on the CTL responses of CO oxidation on Au-doped oxide

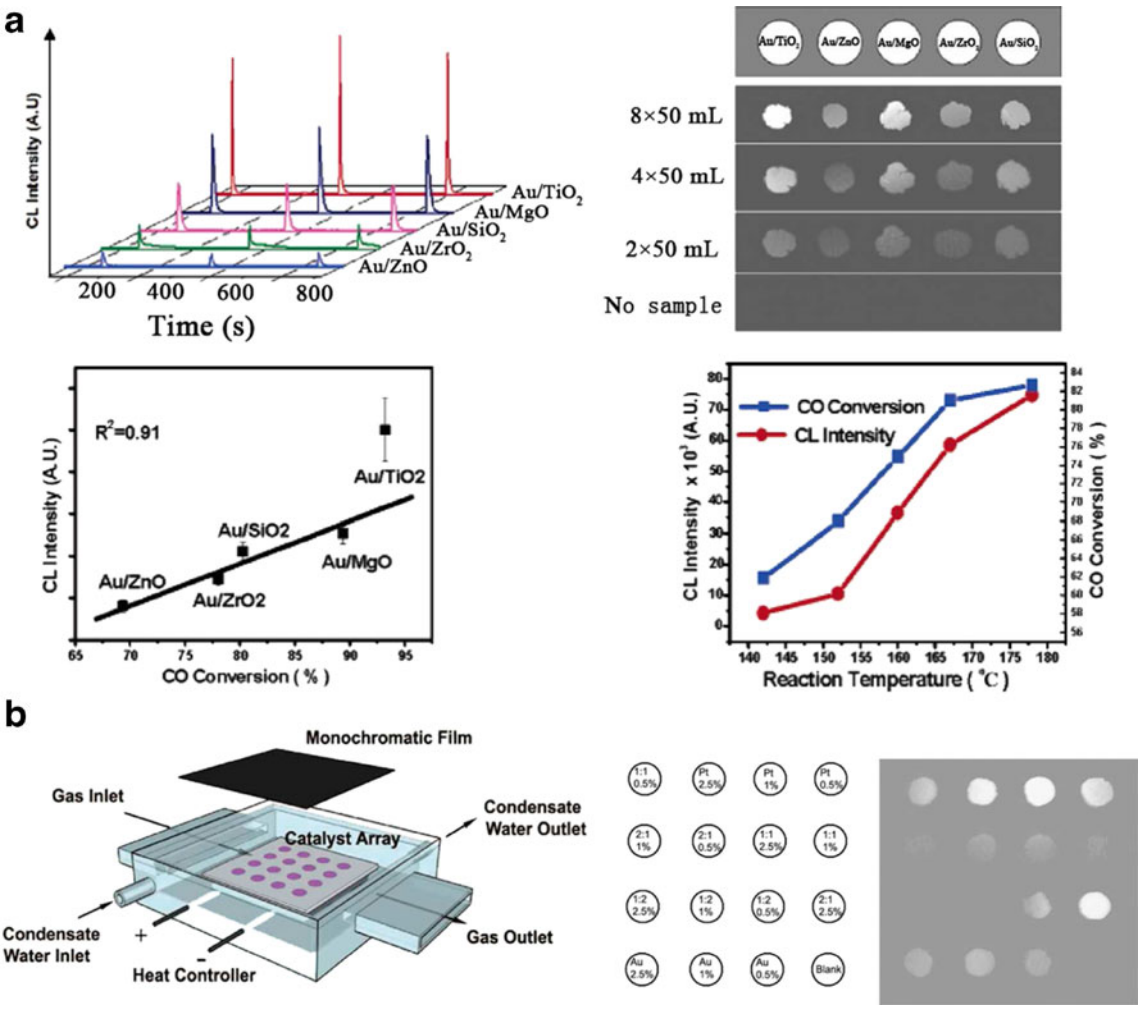

Fig. 13 (**a**) CL responses of CO oxidation on the surface of different oxide-supported gold catalysts, the CTL-based array imaging photographs following a change of CO gas amount, correlation of CTL intensities with CO conversions. (**b**) Schematic of the catalyst screening system and the image obtained from the CTL-based array after exposure to CO gas flow

nanocomposite catalysts [136]. CO was oxidized on these catalysts producing different CTL intensities, and the pattern was imaged simultaneously on a monochromatic film (Fig. 13a). The brightness of the image was in accordance with the catalytic activities of these catalysts. According to the brightness, the order of catalytic activities could be ranked as $Au/TiO_2 > Au/MgO > Au/SiO_2 > Au/ZrO_2 > Au/ZnO$. Thus, the evaluation of catalysts could be rapidly obtained according to the CTL signals recorded on images, which made the sensor array become a rapid and effective tool for catalyst screening.

Thousands of nano-materials have emerged in the field of CTL, which makes the high-throughput screening crucial. Na et al. later integrated a 4×4 array for the high-throughput screening of the catalysts by depositing catalysts on a ceramic chip to record signals of CO oxidation (Fig. 13b) [137]. The catalysts were heterogeneous catalysts with the monometal or bimetal loaded on the substrate of TiO_2, the total loadings of metal were 0.5 %, 1.0 %, and 2.5 %, with atomic ratios of 1:1, 1:2, and 2:1 (Au/Pt). The catalytic activities of these catalysts were evaluated parallelly by both the CTL imaging and the GC method. As a result, the correlation coefficient of the two techniques was 0.914, demonstrating that the CTL imaging technique can be used for the evaluation of the catalytic activities. Coincidentally, de-NO_x catalysts were screened relied on the CTL array images at different working temperatures [138].

In biodiesel production examinations, CTL intensity was proven to be closely related to the amount of medium-strength basic sites of heterogeneous base catalysts [24]. There was also a good match between the CTL screening method and CO_2-temperature-programmed desorption (CO_2-TPD) measurements. This easily operated and quickly responsive CTL-based screen system achieved better understanding of the intrinsic nature of CTL on nano-materials and showed great potential to find expanding applications in discrimination of basic sites of various catalysts.

Conclusions and perspectives

In the past decades, a wide range of applications of CTL-based sensors in chemical analysis have emerged, mainly focused on environmental analysis, commodity quality appraisal, disease diagnosis, and process monitoring. The performance of CTL sensors has been enhanced greatly with the help of a mushroom growth of nano-materials and hyphenated techniques, and CTL-based sensors have exhibited great potential in practical detections. We are looking forward the emergence of CTL-based sensors in the commercial market in the not too distant future.

Despite numerous advancements, CTL-based sensors still have much room for progress. Future possible improvements in CTL-based sensor will probably focus on the following directions:

(1) To establish an accurate cataluminescence theory, developing a method to detect the intermediates produced in the course of catalytic reaction is required.
(2) New materials with better catalytic activity and better selectivity are encouraged for discovery, which can lower the working temperatures to ambient temperatures or even subzero degree.
(3) The miniaturization of sensing system is beneficial to the portability and in situ testing, thus simplifying the equipment of CTL-based sensors but not lowering the detection performance.
(4) Hyphenated techniques sensors or multi-channel transducers combined with CTL-based sensors (array) may enhance the accuracy of detection, especially for the complex molecules.
(5) Only limited types of the biomedical analytes can be detected by the present studies. Diversifying the biological testing samples will be an appealing area in the development of CTL-based sensor.

CTL-based sensors or sensor arrays have made great contributions in chemical analysis, which are expected to further play more significant roles in the future.

Acknowledgments The authors gratefully acknowledge the support from the National Nature Science Foundation of China (21422503, 21475011), Foundation for the Author of National Excellent Doctoral Dissertation of PR China (201221), and the Fundamental Research Funds for the Central Universities.

Compliance with ethical standards

Conflict of interest The authors declare that they have no conflict of interest.

References

1. Breysse M, Claudel B, Faure L, Guenin M, Williams RJ, Wolkenstein T (1976) Chemiluminescence during the catalysis of carbon monoxide oxidation on a thoria surface. J Catal 45(2): 137–144
2. Rufov YN, Kadushin AA, Roginski SZ (1966) Appearance of luminescence when vapour or gas are adsorbed on solids. Dokl Akad Nauk 171(4):905
3. Zhang L, Song H, Su Y, Lv Y (2015) Advances in nanomaterial-assisted cataluminescence and its sensing applications. TrAC Trends Anal Chem 67:107–127
4. Coon VT, Dent AL, Coon DD (1978) Comments on Co oxidation cata-luminescence spectra. J Catal 53(3):328–341
5. Nakagawa M, Fujiwara N, Matsuura Y, Tomiyama T, Yamamoto I, Utsunomiya K, Wada T, Yamashita N, Yamashita Y (1990) An

adsorption luminescence chemical sensor for the measurement of combustible gas-mixtures. Bunseki Kagaku 39(11):797–800
6. Utsunomiya K, Nakagawa M, Sanari N, Kohata M, Tomiyama T, Yamamoto I, Wada T, Yamashita N, Yamashita Y (1995) Continuous determination and discrimination of mixed odor vapors by a new chemiluminescence-based sensor system. Sens Actuators B: Chem 25(1/3):790–793
7. Utsunomiya K, Nakagawa M, Tomiyama T, Yamamoto I, Matsuura Y, Chikamori S, Wada T, Yamashita N, Yamashita Y (1993) Discrimination and determination of gases utilizing adsorption luminescence. Sens Actuators B: Chem 11(1/3):441–445
8. Nakagawa M (1995) A new chemiluminescence-based sensor for discriminating and determining constituents in mixed gases. Sens Actuators B: Chem 29(1/3):94–100
9. Nakagawa M, Kawabata S, Nishiyama K, Utsunomiya K, Yamamoto I, Wada T, Yamashita Y, Yamashita N (1996) Analytical detection system of mixed odor vapors using chemiluminescence-based gas sensor. Sens Actuators B: Chem 34(1/3):334–338
10. Okabayashi T, Fujimoto T, Yamamoto I, Utsunomiya K, Wada T, Yamashita Y, Yamashita N, Nakagawa M (2000) High sensitive hydrocarbon gas sensor utilizing cataluminescence of γ-Al_2O_3 activated with Dy^{3+}. Sens Actuators B: Chem 64(1/3):54–58
11. Okabayashi T, Toda T, Yamamoto I, Utsunomiya K, Yamashita N, Nakagawa M (2001) Temperature-programmed chemiluminescence measurements for discrimination and determination of fragrance. Sens Actuators B: Chem 74(1/3):152–156
12. Zhu Y, Shi J, Zhang Z, Zhang C, Zhang X (2002) Development of a gas sensor utilizing chemiluminescence on nanosized titanium dioxide. Anal Chem 74(1):120–124
13. Magureanu M, Mandache NB, Eloy P, Gaigneaux EM, Parvulescu VI (2005) Plasma-assisted catalysis for volatile organic compounds abatement. Appl Catal B 61(1/2):12–20
14. Hu J, Li W, Zheng C, Hou X (2011) Dielectric barrier discharge in analytical spectrometry. Appl Spectrosc Rev 46(5):368–387
15. Na N, Liu H, Han J, Han F, Liu H, Ouyang J (2012) Plasma-assisted cataluminescence sensor array for gaseous hydrocarbons discrimination. Anal Chem 84(11):4830–4836
16. Han J, Han F, Ouyang J, He L, Zhang Y, Na N (2014) Low temperature CO sensor based on cataluminescence from plasma-assisted catalytic oxidation on Ag doped alkaline-earth nanomaterials. Nanoscale 6(6):3069–3072
17. Yang P, Lau C, Liu X, Lu J (2007) Direct solid-support sample loading for fast cataluminescence determination of acetone in human plasma. Anal Chem 79(22):8476–8485
18. Dickinson TA, White J, Kauer JS, Walt DR (1996) A chemical-detecting system based on a cross-reactive optical sensor array. Nature 382(6593):697–700
19. Nakagawa M, Yamashita N (2005) In: Wolfbeis OS (ed) Frontiers in chemical sensors, 3rd edn. Berlin, Springer
20. Zhou Q, Zhang L, Fan H, Wu L, Lv Y (2010) An ethanol gas sensor using energy transfer cataluminescence on nanosized YVO_4:Eu^{3+} surface. Sens Actuators B: Chem 144(1):192–197
21. Zhang Z, Xu K, Baeyens WRG, Zhang X (2005) An energy-transfer cataluminescence reaction on nanosized catalysts and its application to chemical sensors. Anal Chim Acta 535(1/2):145–152
22. Maestro P, Huguenin D (1995) Industrial applications of rare earths: which way for the end of the century. J Alloys Compd 225(1):520–528
23. Nakagawa M, Yamamoto I, Yamashita N (1998) Detection of organic molecules dissolved in water using a γ-Al_2O_3 chemiluminescence-based sensor. Anal Sci 14(1):209–214
24. Zhang L, Chen Y, He N, Lu C (2014) Acetone cataluminescence as an indicator for evaluation of heterogeneous base catalysts in biodiesel production. Anal Chem 86(1):870–875
25. Shi J, Li J, Zhu Y, Wei F, Zhang X (2002) Nanosized $SrCO_3$-based chemiluminescence sensor for ethanol. Anal Chim Acta 466(1):69–78
26. Wu Y, Zhang S, Na N, Wang X, Zhang X (2007) A novel gaseous ester sensor utilizing chemiluminescence on nano-sized SiO_2. Sens Actuators B: Chem 126(2):461–466
27. Li Z, Xi W, Lu C (2015) Hydrotalcite-assisted cataluminescence: a new approach for sensing mesityl oxide in aldol condensation of acetone. Sens Actuators B: Chem 207:498–503
28. Hu J, Xu K, Jia Y, Lv Y, Li Y, Hou X (2008) Oxidation of ethyl ether on borate glass: chemiluminescence, mechanism, and development of a sensitive gas sensor. Anal Chem 80(21):7964–7969
29. Chu Y, Zhang Q, Li Y, Xu Z, Long W (2014) A cataluminescence sensor for propionaldehyde based on the use of nanosized zirconium dioxide. Microchim Acta 181(9/10):1125–1132
30. Kang C, Tang F, Liu Y, Wu Y, Wang X (2013) A portable gas sensor based on cataluminescence. Luminescence 28(3):313–317
31. Wen F, Zhang S, Na N, Wu Y, Zhang X (2009) Development of a sensitive gas sensor by trapping the analytes on nanomaterials and in situ cataluminescence detection. Sens Actuators B: Chem 141(1):168–173
32. Li S, Li F, Rao Z (2010) A novel and sensitive formaldehyde gas sensor utilizing thermal desorption coupled with cataluminescence. Sens Actuators B: Chem 145(1):78–83
33. Zheng J, Xue Z, Li S, Li S, Rao Z (2012) Development of trichloroethylene gaseous sensor utilizing ZnO-Y_2O_3 as nanocatalyst based on thermal desorption/cataluminescence. Anal Methods 4(9):2791
34. Huang G, Lv Y, Zhang S, Yang C, Zhang X (2005) Development of an aerosol chemiluminescent detector coupled to capillary electrophoresis for saccharide analysis. Anal Chem 77(22):7356–7365
35. Han J, Han F, Ouyang J, Li Q, Na N (2013) Venturi-electrosonic spray ionization cataluminescence sensor array for saccharides detection. Anal Chem 85(16):7738–7744
36. Almasian MR, Na N, Wen F, Zhang S, Zhang X (2010) Development of a plasma-assisted cataluminescence system for benzene, toluene, ethylbenzene, and xylenes analysis. Anal Chem 82(9):3457–3459
37. Han F, Yang Y, Han J, Ouyang J, Na N (2015) Room-temperature cataluminescence from CO oxidation in a non-thermal plasma-assisted catalysis system. J Hazard Mater 293:1–6
38. Albert KJ, Lewis NS, Schauer CL, Sotzing GA, Stitzel SE, Vaid TP, Walt DR (2000) Cross-reactive chemical sensor arrays. Chem Rev 100(7):2595–2626
39. Tisch U, Haick H (2010) Nanomaterials for cross-reactive sensor arrays. MRS Bull 35(10):797–803
40. Palacios MA, Wang Z, Montes VA, Zyryanov GV, Anzenbacher P Jr (2008) Rational design of a minimal size sensor array for metal ion detection. J Am Chem Soc 130(31):10307–10314
41. Lin H, Jang M, Suslick KS (2011) Preoxidation for colorimetric sensor array detection of VOCs. J Am Chem Soc 133(42):16786–16789
42. Rakow NA, Suslick KS (2000) A colorimetric sensor array for odour visualization. Nature 406(6797):710–713
43. Na N, Zhang S, Wang S, Zhang X (2006) A catalytic nanomaterial-based optical chemo-sensor array. J Am Chem Soc 128(45):14420–14421
44. Kong H, Zhang S, Na N, Liu D, Zhang X (2009) Recognition of organic compounds in aqueous solutions by chemiluminescence on an array of catalytic nanoparticles. Analyst 134(12):2441–2446
45. Liu B, Kong H, Luo A (2014) A cataluminescence-based vapor-sensitive sensor array for discriminating flammable liquid vapors. Talanta 121:43–49
46. Zhang R, Cao X, Liu Y, Chang X (2013) Development of a simple cataluminescence sensor system for detecting and discriminating volatile organic compounds at different concentrations. Anal Chem 85(8):3802–3806

47. Chen J, Cao X, Xing R, Xu L, Liu Y, Zeng J (2013) A sensor system for identifying ether vapors based on extracting two-stage cataluminescence signals. Acta Chim Sin 71(10):1421
48. Liu D, Liu M, Liu G, Zhang S, Wu Y, Zhang X (2009) Dual-channel sensing of volatile organic compounds with semiconducting nanoparticles. Anal Chem 82(1):66–68
49. Lv Y, Zhang S, Liu G, Huang M, Zhang X (2005) Development of a detector for liquid chromatography based on aerosol chemiluminescence on porous alumina. Anal Chem 77(5):1518–1525
50. Zeng J, Cao X, Liu Y, Chen J, Ren K (2014) A single cataluminescence sensor for wine identification by luminescent response profiles. Anal Methods 6(8):2633–2641
51. Zhang R, Cao X, Liu Y, Chang X (2011) A new method for identifying compounds by luminescent response profiles on a cataluminescence based sensor. Anal Chem 83(23):8975–8983
52. Wu Y, Wen F, Liu D, Kong H, Zhang C, Zhang S (2011) Analysis of 2-propanol in exhaled breath using in situ enrichment and cataluminescence detection. Luminescence 26(2):125–129
53. Yang H, Xing Z, Zhou K (2014) A sensitive formaldehyde sensor based on cataluminescence coupled with thermal desorption. Appl Mech Mater 670/671:1163–1166
54. Zhou K, Li X, Su D, Yang H, Shen X (2012) A rapid and sensitive acetone gas sensor utilizing thermal desorption coupled with cataluminescence on nano-Cr_4TiO_8. Adv Mater Res 468/471: 217–220
55. Zheng J, Zhang W, Cao J, Su X, Li S, Hu S, Li S, Rao Z (2014) A novel and highly sensitive gaseous n-hexane sensor based on thermal desorption/cataluminescence. RSC Adv 4(41):21644
56. Xia H, Zhou R, Zheng C, Wu P, Tian Y, Hou X (2013) Solution-free, in situ preparation of nano/micro CuO/ZnO in dielectric barrier discharge for sensitive cataluminescence sensing of acetic acid. Analyst 138(13):3687–3691
57. Li S, Zheng J, Zhang W, Cao J, Rao Z (2013) Molecular recognition and quantitative analysis of xylene isomers utilizing cataluminescence sensor array. Analyst 138(3):916–920
58. Xu S, Zhang L, Zhang X, He C, Lv Y (2011) Synthesis of Ag_2Se nanomaterial by electrodeposition and its application as cataluminescence gas sensor material for carbon tetrachloride. Sens Actuators B: Chem 155(1):311–316
59. Wang Y, Li B, Wang Q, Shou Z (2015) Development of a cataluminescence sensor for detecting benzene based on magnesium silicate hollow spheres. Luminescence 30(5):619–624
60. Yu C, Liu G, Zuo B, Tang Y, Zhang T (2008) A novel gaseous pinacolyl alcohol sensor utilizing cataluminescence on alumina nanowires prepared by supercritical fluid drying. Anal Chim Acta 618(2):204–209
61. Li Z, Xi W, Lu C (2015) Hydrotalcite-supported gold nanoparticle catalysts as a low temperature cataluminescence sensing platform. Sens Actuators B: Chem 219:354–360
62. Cao X, Zhang Z, Zhang X (2004) A novel gaseous acetaldehyde sensor utilizing cataluminescence on nanosized $BaCO_3$. Sens Actuators B: Chem 99(1):30–35
63. Wang Q, Li B, Wang Y, Shou Z, Shi G (2015) Sensitive and selective cataluminescence-based sensor system for acetone and diethyl ether determination. Luminescence 30(3):318–324
64. Sha W, Gu P, Zhang B, Zheng C (2014) A cataluminescence sensor system for diethyl ether based on CdO nanostructure. Meas Sci Technol 25(8):085102
65. Jiao X, Zhang L, Lv Y, Su Y (2013) A new alcohols sensor based on cataluminescence on nano-CdS. Sens Actuators B: Chem 186: 750–754
66. Xuan Y, Hu J, Xu K, Hou X, Lv Y (2009) Development of sensitive carbon disulfide sensor by using its cataluminescence on nanosized-CeO_2. Sens Actuators B: Chem 136(1):218–223
67. Liu H, Zhang Y, Zhen Y, Ma Y, Zuo W (2014) A 1,2-propylene oxide sensor utilizing cataluminescence on CeO_2 nanoparticles. Luminescence 29(8):1183–1187
68. Xie X, Li Y, Liu ZQ, Haruta M, Shen W (2009) Low-temperature oxidation of CO catalysed by Co_3O_4 nanorods. Nature 458(7239): 746–749
69. Teng F, Yao W, Zheng Y, Ma Y, Teng Y, Xu T, Liang S, Zhu Y (2008) Synthesis of flower-like CuO nanostructures as a sensitive sensor for catalysis. Sens Actuators B: Chem 134(2):761–768
70. Zhang Z, Jiang H, Xing Z, Zhang X (2004) A highly selective chemiluminescent H_2S sensor. Sens Actuators B: Chem 102(1): 155–161
71. Tao Y, Cao X, Peng Y, Liu Y, Zhang R (2011) Cataluminescence sensor for gaseous acetic acid using a thin film of In_2O_3. Microchim Acta 176(3/4):485–491
72. Teng F, Xu T, Teng Y, Liang S, Gauge B, Lin J, Yao W, Zong R, Zhu Y, Zheng Y (2008) A CL mode detector for rapid catalyst selection and environmental detection fabricated by perovskite nanoparticles. Environ Sci Technol 42(10):3886–3892
73. Teng F, Yao W, Zhu Y, Chen M, Wang R, S-i M, Meng D (2009) Correlation cataluminescence (CTL) property with reactivity of hydrothermally synthesized $La_{0.8}Sr_{0.2}MnO_3$ cubes and CTL as a rapid mode of screening catalyst. J Phys Chem C 113(8):3089–3095
74. Shi J (2003) Determination of NH_3 gas by combination of nanosized $LaCoO_3$ converter with chemiluminescence detector. Talanta 61(2):157–164
75. Tang L, Li Y, Xu K, Hou X, Lv Y (2008) Sensitive and selective acetone sensor based on its cataluminescence from nano-La_2O_3 surface. Sens Actuators B: Chem 132(1):243–249
76. Wu C, Cao X, Wen Q, Wang Z, Gao Q, Zhu H (2009) A vinyl acetate sensor based on cataluminescence on MgO nanoparticles. Talanta 79(5):1223–1227
77. Tao Y, Cao X, Peng Y, Liu Y (2010) A novel cataluminescence gas sensor based on MgO thin film. Sens Actuators B: Chem 148(1):292–297
78. Zhang L, Zhou Q, Liu Z, Hou X, Li Y, Lv Y (2009) Novel Mn_3O_4 micro-octahedra: promising cataluminescence sensing material for acetone. Chem Mater 21(21):5066–5071
79. Zhang L, Wang S, Lu C (2015) Detection of oxygen vacancies in oxides by defect-dependent cataluminescence. Anal Chem 87(14): 7313–7320
80. Liu G, Zhu Y, Zhang X, Xu B (2002) Chemiluminescence determination of chlorinated volatile organic compounds by conversion on nanometer TiO_2. Anal Chem 74(24):6279–6284
81. Zhang H, Zhang L, Hu J, Cai P, Lv Y (2010) A cataluminescence gas sensor based on nanosized V_2O_5 for tert-butyl mercaptan. Talanta 82(2):733–738
82. Zhou K, Ji X, Zhang N, Zhang X (2006) On-line monitoring of formaldehyde in air by cataluminescence-based gas sensor. Sens Actuators B: Chem 119(2):392–397
83. Zhang Z, Xu K, Xing Z, Zhang X (2005) A nanosized Y_2O_3-based catalytic chemiluminescent sensor for trimethylamine. Talanta 65(4):913–917
84. Rao Z, Liu L, Xie J, Zeng Y (2008) Development of a benzene vapour sensor utilizing chemiluminescence on Y_2O_3. Luminescence 23(3):163–168
85. Wu Y, Zhang S, Wang X, Na N, Zhang Z (2008) Development of a benzaldehyde sensor utilizing chemiluminescence on nanosized Y_2O_3. Luminescence 23(6):376–380
86. Cao X, Tao Y, Li L, Liu Y, Peng Y, Li J (2011) An ethyl acetate sensor utilizing cataluminescence on Y_2O_3 nanoparticles. Luminescence 26(1):5–9
87. Gu C, Xing Z, Cai X, Zhang J, Gao B, Zhou K (2013) Determination of dimethyl ether in air by cataluminescence-based gas sensor. Adv Mater Res 739:537–542

88. Tang H, Li Y, Zheng C, Ye J, Hou X, Lv Y (2007) An ethanol sensor based on cataluminescence on ZnO nanoparticles. Talanta 72(4):1593–1597
89. Cai P, Song H, Zhang L, Lv Y (2012) Enhanced cataluminescence sensing characteristics of ethanol on hierarchical spheres ZnO. Sens Actuators B: Chem 173:93–99
90. Cao X, Wu W, Chen N, Peng Y, Liu Y (2009) An ether sensor utilizing cataluminescence on nanosized $ZnWO_4$. Sens Actuators B: Chem 137(1):83–87
91. Luo L, Chen H, Zhang L, Xu K, Lv Y (2009) A cataluminescence gas sensor for carbon tetrachloride based on nanosized ZnS. Anal Chim Acta 635(2):183–187
92. Yu C, Liu G, Zuo B, Tang R (2009) A novel gaseous dimethylamine sensor utilizing cataluminescence on zirconia nanoparticles. Luminescence 24(5):282–289
93. Zhang Z, Zhang C, Zhang X (2002) Development of a chemiluminescence ethanol sensor based on nanosized. ZrO2 Anal 127(6):792–796
94. Cao X, Feng G, Gao H, Luo X, Lu H (2005) Nanosized γ-Al_2O_3+ Nd_2O_3-based cataluminescence sensor for ethylene dichloride. Luminescence 20(3):104–108
95. Okabayashi T, Ozaki M, Nakagawa M (2011) Detection method of isoflurane vapor using a cataluminescence-based gas sensor. Proc Eng 25:1093–1096
96. Cao X, Dai H, Chen S, Zeng J, Zhang K, Sun Y (2013) A high selective cataluminescence sensor for the determination of tetrahydrofuran vapor. Meas Sci Technol 24(2):025103
97. Liu Y, Tang F, Kang C, Cao X (2012) Detection of hydrogen sulphide using cataluminescence sensors based on alkaline-earth metal salts. Luminescence 27(4):274–278
98. Guo Z, Jiang Z, Chen X, Sun B, Li M, Liu J, Huang X (2011) Novel cocoon-like Au/La_2O_3 nanomaterials: synthesis and their ultra-enhanced cataluminescence performance to volatile organic compounds. J Mater Chem 21(6):1874–1879
99. Li B, Zhang Y, Liu J, Xie X, Zou D, Li M, Liu J (2014) Sensitive and selective system of benzene detection based on a cataluminescence sensor. Luminescence 29(4):332–337
100. Cao H, Zhang L, Liu X, Zhang S, Liang Y, Zhang X (2007) Catalytic chemiluminescence properties of boehmite "nanococoons". Appl Phys Lett 90(19):193105–193113
101. Sun Z, Zhang X, Han B, Wu Y, An G, Liu Z, Miao S, Miao Z (2007) Coating carbon nanotubes with metal oxides in a supercritical carbon dioxide–ethanol solution. Carbon 45(13):2589–2596
102. Sun Z, Yuan H, Liu Z, Han B, Zhang X (2005) A highly efficient chemical sensor material for H_2S: α-Fe_2O_3 nanotubes fabricated using carbon nanotube templates. Adv Mater 17(24):2993–2997
103. Zeng B, Zhang L, Wan X, Song H, Lv Y (2015) Fabrication of α-Fe_2O_3/g-C_3N_4 composites for cataluminescence sensing of H_2S. Sens Actuators B: Chem 211:370–376
104. Xu S, Tang L, Bi C, Wang X, Lv Y (2010) A cataluminescence gas sensor for ammonium sulfide based on Fe_3O_4-carbon nanotubes composite. Luminescence 25(4):294–299
105. Zhou L (2013) An automobile exhaust sensor utilizing cataluminescence on nanosized Fe_3O_4/SiO_2. Appl Mech Mater 288:121–124
106. Cai P, Bai W, Zhang L, Song H, Su Y, Lv Y (2012) Hierarchical hollow microsphere and flower-like indium oxide: controllable synthesis and application as H_2S cataluminescence sensing materials. Mater Res Bull 47(9):2212–2218
107. Xu L, Song H, Hu J, Lv Y, Xu K (2012) A cataluminescence gas sensor for triethylamine based on nanosized LaF_3-CeO_2. Sens Actuators B: Chem 169:261–266
108. Teng F, Gaugeu B, Liang S, Zhu Y (2007) Preparation of $LaSrCuO_4$ nanowires by carbon nanotubes and their catalytic and chemiluminescence properties for CO oxidation. Appl Catal A 328(2):156–162
109. Teng F, Xu T, Liang S, Buergen G, Yao W, Zhu Y (2008) Synthesis of hollow Mn_3O_4-in-Co_3O_4 magnetic microspheres and its chemiluminescence and catalytic properties. Catal Commun 9(6):1119–1124
110. Chu Y, Zhang Q, Zhang W, Zhang G, Zhu S (2014) Highly sensitive dimethyl ether gas sensor utilizing cataluminescence on nanosized MgO/In_2O_3. Meas Sci Technol 25(8):085105–085117
111. Jia Y, Zhang H, Wu L, Lv Y, Hou X (2010) A new cataluminescence sensor for carbon tetrachloride using its catalytic reduction by hydrogen on palladium/carbon surface. Microchem J 95(2):359–365
112. Wang Y, Cao X, Li J, Chen N (2011) A new cataluminescence gas sensor based on SiO_2 nanotubes fabricated using carbon nanotube templates. Talanta 84(3):977–982
113. Shi G, Sun B, Jin Z, Liu J, Li M (2012) Synthesis of SiO_2/Fe_3O_4 nanomaterial and its application as cataluminescence gas sensor material for ether. Sens Actuators B: Chem 171/172:699–704
114. An G, Na N, Zhang X, Miao Z, Miao S, Ding K, Liu Z (2007) SnO_2/carbon nanotube nanocomposites synthesized in supercritical fluids: highly efficient materials for use as a chemical sensor and as the anode of a lithium-ion battery. Nanotechnology 18(43): 435707
115. Yu L, Zhang L, Song H, Jiang X, Lv Y (2014) Hierarchical SnO_2 architectures: controllable growth on graphene by atmospheric pressure chemical vapour deposition and application in cataluminescence gas sensor. CrystEngComm 16(16):3331
116. Yu L, Song H, Tang Y, Zhang L, Lv Y (2014) Controllable deposition of ZnO-doped SnO_2 nanowires on Au/graphene and their application in cataluminescence sensing for alcohols and ketones. Sens Actuators B: Chem 203:726–735
117. Song H, Zhang L, He C, Qu Y, Tian Y, Lv Y (2011) Graphene sheets decorated with SnO_2 nanoparticles: in situ synthesis and highly efficient materials for cataluminescence gas sensors. J Mater Chem 21(16):5972–5977
118. Miao Z, Wu Y, Zhang X, Liu Z, Han B, Ding K, An G (2007) Large-scale production of self-assembled SnO_2 nanospheres and their application in high-performance chemiluminescence sensors for hydrogen sulfide gas. J Mater Chem 17(18):1791–1796
119. Zhang Q, Meng F, Zha L, Wang X, Zhang G (2015) A sensitive cataluminescence-based sensor using a $SrCO_3$/graphene composite for n-propanol. RSC Adv 5(71):57482–57489
120. Sha W, Ni S, Zheng C (2015) Development of cataluminescence sensor system for benzene and toluene determination. Sens Actuators B: Chem 209:297–305
121. Weng Y, Zhang L, Zhu W, Lv Y (2015) One-step facile synthesis of coral-like Zn-doped SnO_2 and its cataluminescence sensing of 2-butanone. J Mater Chem A 3(13):7132–7138
122. Sun Z, Zhang X, Na N, Liu Z, Han B, An G (2006) Synthesis of ZrO_2-carbon nanotube composites and their application as chemiluminescent sensor material for ethanol. J Phys Chem B 110(27): 13410–13414
123. Zhang R, Cao X, Liu Y, Peng Y (2010) A highly sensitive and selective dimethyl ether sensor based on cataluminescence. Talanta 82(2):728–732
124. Zhang L, Rong W, Chen Y, Lu C, Zhao L (2014) A novel acetone sensor utilizing cataluminescence on layered double oxide. Sens Actuators B: Chem 205:82–87
125. Wan X, Wu L, Zhang L, Song H, Lv Y (2015) Novel metal-organic frameworks-based hydrogen sulfide cataluminescence sensors. Sens Actuators B: Chem 220:614–621
126. Wan X, Song H, Zhao D, Zhang L, Lv Y (2014) A Y-doped metal-organic framework-based cataluminescence gas sensor for isobutanol. Sens Actuators B: Chem 201:413–419

127. Yang N, Song H, Wan X, Fan X, Su Y, Lv Y (2015) A metal (Co)-organic framework-based chemiluminescence system for selective detection of L-cysteine. Analyst 140(8):2656–2663
128. Yang P, Lau C, Liang J, Lu J, Liu X (2007) Zeolite-based cataluminescence sensor for the selective detection of acetaldehyde. Luminescence 22(5):473–479
129. Yang P, Ye X, Lau C, Li Z, Liu X, Lu J (2007) Design of efficient zeolite sensor materials for n-hexane. Anal Chem 79(4):1425–1432
130. Wu Y, Na N, Zhang S, Wang X, Liu D, Zhang X (2009) Discrimination and identification of flavors with catalytic nanomaterial-based optical chemosensor array. Anal Chem 81(3):961–966
131. Sha W, Cui D, Li B, Wang Q, Wang Y, Zheng C (2014) A portable embedded drug precursor gas detection and identification device based on cataluminescence-based sensor array. Sens Actuators B: Chem 200:132–139
132. Zhang C, Suslick KS (2005) A colorimetric sensor array for organics in water. J Am Chem Soc 127(33):11548–11549
133. Niu W, Kong H, Wang H, Zhang Y, Zhang S, Zhang X (2012) A chemiluminescence sensor array for discriminating natural sugars and artificial sweeteners. Anal Bioanal Chem 402(1):389–395
134. Kong H, Liu D, Zhang S, Zhang X (2011) Protein sensing and cell discrimination using a sensor array based on nanomaterial-assisted chemiluminescence. Anal Chem 83(6):1867–1870
135. Kong H, Wang H, Zhang S, Zhang X (2011) A thermochemiluminescence array for recognition of protein subtypes and their denatured shapes. Analyst 136(18):3643–3648
136. Wang X, Na N, Zhang S, Wu Y, Zhang X (2007) Rapid screening of gold catalysts by chemiluminescence-based array imaging. J Am Chem Soc 129(19):6062–6063
137. Na N, Zhang S, Wang X, Zhang X (2009) Cataluminescence-based array imaging for high-throughput screening of heterogeneous catalysts. Anal Chem 81(6):2092–2097
138. Wu L, Zhang Y, Zhang S, Zhang X (2012) Development of a cataluminescence-based method for rapid screening of de-NO_x catalysts. Anal Methods 4(8):2218